CHROMOSPHERIC STRUCTURE OF THE K-TYPE COMPONENT OF ZETA AURIGAE

O. C. WILSON AND HELMUT A. ABT*
MOUNT WILSON AND PALOMAR OBSERVATORIES
CARNEGIE INSTITUTION OF WASHINGTON
CALIFORNIA INSTITUTE OF TECHNOLOGY
Received July 30, 1953

ABSTRACT

Spectrograms of 10 A/mm dispersion taken during the 1947–1948 eclipse have been measured for line intensities and for radial velocities, and the results are compared with those obtained previously for the 1939–1940 eclipse. Egress of 1947–1948 is found to be quite similar to ingress and egress of 1939–1940; ingress at the more recent eclipse differs, however, from the other three transits in the direction of a considerably slower gradient, particularly at the greater chromospheric heights. This effect is found from lines of all types. However, ingress of 1947–1948 is not distinguishable from the other transits in the values of any of the derived parameters: excitation temperature, turbulent velocity, or degree of ionization.

It is shown that the apparent rise of $\Delta\lambda_D$ with height found in 1939–1940 is really due to a systematic difference in this quantity between the neutral and ionized lines. Ions indicate slightly higher turbulent velocities than do neutral atoms. The excitation temperature increases with height at about the same rate as indicated by the earlier results.

Ionization in the chromosphere is studied in some detail, and Strömgren's theory of the penetration of ionizing radiation from the B star into the chromosphere of the K star is applied to the problem. The outcome is that it appears impossible to account for the spectroscopic phenomena on the basis of a smooth distribution of the chromospheric material. In fact, it is necessary to assume that the matter occurs in condensations of rather small size (thickness of the order of 10^3 km) and high density (log $n[H] = 13.8$) in order to keep the ionization at the required level and to avoid discordance with the solar abundance ratios. The model is in accord with all but one of the observed spectroscopic features, as well as with the recent interpretation of the photometric eclipse by Roach and Wood.

I. INTRODUCTION

In eclipsing binaries of which one component is a giant or supergiant star of large size and low surface temperature, while the other component possesses opposite characteristics, the eclipses of the small star by its companion offer an opportunity to determine the chromospheric structure of the large, cool star. At present, four systems of this type are known: Zeta Aurigae, 31 Cygni, 32 Cygni, and VV Cephei.[1] Zeta Aurigae has been known longer and investigated more completely than the others.

The period of Zeta Aurigae is about 972 days; hence favorable eclipses (in the sense that the star is observable throughout the night) occur every 8 years. The eclipse of December, 1939—January, 1940, was observed spectroscopically by one of the authors,[2] and more extensive observations were obtained of the 1947–1948 eclipse. In this paper the results of the more recent eclipse are derived and compared with those of the earlier one.

With a few exceptions noted in the text, the methods of measurement, reduction, and computation used in the earlier work have been employed for the more recent material. In fact, most of the spectrograms obtained in 1947–1948 were taken with the same

* Now at Yerkes Observatory, Williams Bay, Wisconsin.

[1] A semiquantitative comparison of the eclipse phenomena of these stars has recently been given by D. B. McLaughlin, *Pub. A.S.P.*, **64**, 173, 1952.

[2] O. C. Wilson, *Ap. J.*, **107**, 137, 1948.

equipment and on the same type of emulsion (Eastman 103-O) as were those of 1939–1940. For details, therefore, the reader is referred to the published report of the earlier eclipse.[2]

The principal advantage of the newer results lies in the greater range of atmospheric height covered in the 1947–1948 observations. A number of the spectrograms have been measured for the velocities, as well as the intensities, of the chromospheric lines, and these will be discussed in the appropriate place; also a few minor numerical errors discovered in the earlier work have been corrected. In the last half of the paper a chromospheric model is developed which is consistent with most of the spectroscopic observations.

II. OBSERVATIONS

For convenience, all the spectrograms utilized for both eclipses are listed in Table 1, which is self-explanatory except for the columns headed "Δt" and "Height." For these items we have arbitrarily adopted as zero points the times corresponding to what would be second and third contacts in a purely geometrical eclipse. These times have been obtained from Wood's epochs of minimum,[3] JD 2429637.10 and JD 2432553.67 for 1939 and 1947, respectively, and Pettit's[4] value for the duration of totality, 36.80 days. With Harper's elements,[5] modified only by the use of Wood's period of 972.16 days, and a mass ratio $M_K/M_B = 2.00$, the resulting conversion factor between time and height in the K star's atmosphere is 7.23×10^6 km/day and is the same for ingress and egress to within less than half a per cent. It should be noted that the heights given in Table 1 for the 1939–1940 spectrograms differ from those previously published because of the change in zero point.

III. SPECTROPHOTOMETRY

The same criteria of choice of lines for intensity measurement were applied to the 1947–1948 material as had been used previously.[2] Some lines of *Fe* II with unkown *f*-value have been measured on the plates of both eclipses, for reasons which will appear later; in other cases the *f*-values were taken from known sources.[6] Equivalent widths of the lines were determined as described previously,[2] and the logarithms of the equivalent widths of the metallic lines, reduced to a mean wave length of 3700 A, are given in Table 2.

Measures of equivalent width of *Ca* I, *Ca* II, and *H* lines are in Table 3, together with corresponding values of log N, which were read from theoretical curves of growth.[7] Values of $\Delta\lambda_D$ appropriate to the height were used for *Ca* I and *Ca* II, while a constant value of $\Delta\lambda_D = 0.15$ A was employed for all the *H* lines. For a few of the strongest *Ca* II lines it was necessary to free the chromospheric component from the effect of the normal K-spectrum line by means of Wilson's equation (3).[2] For convenience, revised values of log N for *Ca* I, *Ca* II, and *H* for the 1939–1940 eclipse are given in Table 4, with the heights corresponding to the usage of this paper. Table 4 thus replaces Wilson's Table 7.[2]

[3] *Ap. J.*, **114**, 505, 1951.

[4] *Pub. A.S.P.*, **60**, 102, 1948.

[5] *Dom. Ap. Obs. Victoria*, **3**, 151, 1924.

[6] *Fe* I: R. B. and A. S. King, *Ap. J.*, **87**, 24, 1938. *Ni* I: R. B. King, *Ap. J.*, **108**, 87, 1948. *Cr* I: A. J. Hill and R. B. King, *J. Opt. Soc. Amer.*, **41**, 315, 1951. *Ca* I, *Ca* II: P. Wellmann, *Veröff. Sternw. Berlin-Babelsberg*, **12**, Part IV, 56, 1939. *Ti* II: R. B. King, *Ap. J.*, **94**, 27, 1941. *H* I: D. H. Menzel and C. J. Pekeris, *M.N.*, **96**, 77, 1935. Miscellaneous solar values: H. H. Lane, *Harvard Ann.*, **105**, 69, 1937.

[7] As in n. 2, N in this paper indicates a total or integrated number of particles along a ray. The symbol n is restricted to number per cubic centimeter.

TABLE 1

SPECTROGRAMS, TIMES OF OBSERVATION, AND CALCULATED HEIGHTS

1947–1948 ECLIPSE

Plates (Coudé)	Date	P.S.T.*	JD 2432000+	Δt (Days)	Height (10^6 Km)
4992, 4994	Dec. 8	13:18	528.89	6.38	46.1
4995, 4996	Dec. 9	8:12	529.68	5.59	40.4
4999, 5000	Dec. 10	12:11	530.84	4.42	32.0
5001, 5002	Dec. 11	8:51	531.70	3.56	25.8
5004	Dec. 11	13:42	531.90	3.36	24.3
5006, 5008	Dec. 12	12:00	532.83	2.44	17.6
5010, 5011	Dec. 13	7:57	533.67	1.60	11.6
5014, 5015	Dec. 13	15:01	533.96	1.31	9.4
5019	Dec. 15	8:27	535.69	Totality	
5026	Dec. 22	9:00	542.71	Totality	
5028†	Dec. 22	13:22	542.89	Totality	
5059	Jan. 20	6:22	571.60	Totality	
5071	Jan. 22	7:52	573.66	1.60	11.5
5074	Jan. 23	6:01	574.58	2.52	18.2
5078	Jan. 24	6:14	575.59	3.53	25.5
5080	Jan. 24	13:14	575.88	3.82	27.6
5083	Jan. 26	11:11	577.80	5.74	41.5
5084	Jan. 27	9:01	578.71	6.64	48.0
5085	Jan. 28	5:51	579.58	7.51	54.3

* Time counted from noon of the day listed.

† Red-sensitive plate taken with the 114-inch camera.

1939–1940 ECLIPSE

Plate (Coudé)	Date	P.S.T.*	JD 2429000+	Δt (Days)	Height (10^6 Km)
2181, 2183	Dec. 16	11:38	614.82	3.88	28.0
2185, 2188	Dec. 17	11:36	615.82	2.88	20.8
2191, 2192, 2194	Dec. 18	9:23	616.72	1.98	14.3
2199	Dec. 19	9:53	617.74	0.96	6.9
2202	Dec. 19	12:55	617.87	Totality	
2205	Dec. 19	15:32	618.78	Totality	
2243	Jan. 26	9:11	655.74	Totality	
2245	Jan. 27	7:45	656.66	1.16	8.4
2248	Jan. 28	6:50	657.62	2.12	15.3
2252, 2253	Jan. 29	9:30	658.73	3.23	23.3
2254	Jan. 30	9:52	659.74	4.24	30.7
2255	Jan. 31	10:15	660.76	5.26	38.0

TABLE 2

Values of - Log W $\frac{3700}{\lambda}$

El. Mult. λ	Log gf	Ce 4992 4994	4995 4996	4999 5000	5001 5002	5004	5006 5008	5010 5011	5014 5015	5071	5074	5078	5080	5083	5084	5085
Fe I																
$a^5D-z^5P^o$																
3440.6	2.20						0.81	0.53		0.62	1.05	1.78				
3441.3	1.82						0.98	0.59		0.78						
3443.9	1.27															
3465.9	1.89					1.04	0.73	0.55	0.49	0.47	1.15	1.53	1.82			
3475.5	1.88						0.77	0.52	0.34							
3490.6	1.73								0.49	0.71		1.05				
$a^5F-z^3G^o$																
3521.3	2.42							0.82	0.52	1.30						
3526.2	2.14							0.76	0.54	1.03						
3565.4	3.14					0.98	0.81	0.64	0.53	0.67	1.45					
3570.1	3.35				0.73	0.72	0.68	0.54	0.41	0.59	0.79	1.56				
$a^5F-z^5G^o$																
3587.0	2.58				1.03	1.03	0.90	0.65	0.60	0.70	1.19					
3589.1	1.70							1.29	1.20							
3608.9	3.12				1.07	0.91	0.80	0.62	0.56	0.80	1.43					
3618.4	3.30				1.27	0.85	0.75	0.58	0.47	0.71	1.19					
3631.5	3.18			1.03	0.74	0.69	0.59	0.46	0.46	0.55	0.83	1.11	1.37			
3647.8	3.14					0.96	0.80	0.56	0.42	0.67						
$a^5D-z^5F^o$																
3649.5	0.43							1.23	1.28							
3679.9	1.78						0.99	0.60	0.63	0.75	1.48					
3683.0	0.89				0.88	0.87	0.77	0.68	0.69							
3705.6	1.98						0.90	0.64	0.51	0.56	1.62					

TABLE 2 (Cont'd)

El. Mult. λ	Log gf	Ce 4992 4994	4995 4996	4999 5000	5001 5002	5004	5006 5008	5010 5011	5014 5015	5071	5074	5078	5080	5083	5084	5085
3707.8	1.01							1.09	0.81							
3719.9	2.72				0.93	0.73	0.56	0.43	0.30	0.41	0.86	1.66				
3722.6	1.98					1.05	0.81	0.56	0.47	0.79						
3733.3	1.83						0.94	0.84	0.64	0.81	1.40					
3737.1	2.59				0.76	0.70	0.56	0.34	0.34	0.46	1.00	1.47	1.56			
3748.3	2.15				0.89	0.89	0.86	0.57	0.56	0.57	1.01	1.31	1.39			
$a^5F\text{-}y^5F^o$																
3687.5	2.63						1.05	0.80	0.60	0.96	1.17					
3709.2	2.78						1.02	0.71	0.56	0.83						
3727.6	2.76							0.57	0.50	0.66						
3734.9	3.67					0.56	0.43	0.36	0.38	0.59	0.84	1.31				
3743.3	2.59						1.12	0.75	0.63	1.00						
3749.5	3.50				0.75	0.59	0.56	0.35	0.34	0.55	0.83	1.14	1.31			
3758.2	3.33				0.96	0.78	0.71	0.53	0.57	0.57	1.17					
3763.8	3.10				1.06	0.93	0.82	0.51	0.59	0.67	1.22					
3767.2	2.93				1.13	1.09	0.95	0.65	0.54	0.67	1.08					
3787.9	2.52				1.32	1.29	1.18	0.81	0.72	1.01	1.27					
3795.0	2.61				1.27	1.07	1.10	0.70	0.60	0.96						
$a^3F\text{-}y^3D^o$																
3815.8	3.72				1.23	1.07	0.88	0.60	0.45	0.59	1.21					
3827.8	3.58				1.18	1.14	0.99	0.68	0.54	0.61	1.62					
3841.0	3.41				1.01	1.20	1.02	0.71	0.67	0.98						
3888.5	2.93															
3903.0	3.11					1.40		0.67	0.62	0.74						
$a^5F\text{-}y^5D^o$																
3820.4	3.49				0.93	0.81	0.63	0.47	0.42	0.50	0.87	1.24				
3825.9	3.28				1.04	0.97	0.78	0.51	0.46	0.47	1.03					
3834.2	3.06			1.60	1.14	1.02	0.91	0.54	0.59	0.64	1.11	1.45				
3840.4	2.78				1.07	1.07	0.88	0.65	0.57	0.77	1.32					
3850.0	2.53					1.35	1.18	0.92	0.83	1.04						
3865.5	2.44						1.40	0.97	0.71	0.91						
3872.5	2.46						1.03	0.88	0.76	1.08						

TABLE 2 (Cont'd)

3878.0	2.50			1.35	1.00	0.89	0.73	1.05	
3887.0	2.36			1.42	1.01	0.80	0.73	1.12	
3998.0	1.54						0.95		
3917.2	1.47					1.58	1.16		
3940.9	1.08					1.39	1.28		
a^5D-z^5D^o									
3824.4	1.94	1.29	1.39	1.10	0.70	0.62	0.69	1.25	
3856.4	1.98		0.96	0.84	0.71	0.54	0.71		
3859.9	2.54	0.91	0.92	0.67	0.45	0.43	0.60	0.96	
3878.6	1.84		1.19	0.97	0.68	0.53	0.77	1.40	
3886.3	2.14		1.14	0.73	0.74	0.57	0.67	1.15	
3895.7	1.58		1.09	1.00	0.83	0.65	0.92		
3899.7	1.74		1.29	1.00	0.80	0.58	0.94		
3906.5	1.15				0.96	0.78	1.04		
3920.3	1.54			1.20	0.80	0.62	0.97		
3922.9	1.70			1.02	0.72	0.65	0.84		
3927.9	1.71		1.39	1.08	0.73	0.58	0.95		
3930.3	1.79			1.05	0.73	0.56	0.88		
a^3F-y^3F^o									
4045.8	3.78	0.85	0.91	0.82	0.51	0.43		0.93	1.21
4063.6	3.54	1.20	0.90	0.93	0.62	0.50		1.15	
4071.8	3.43	1.21	1.09	0.80	0.61	0.52		1.10	1.20
Ni I									
a^3D-z^3F^o									
3414.8	6.90				1.05	0.60	0.51	0.87	1.61
3458.5	6.55				1.02	0.87	0.63	1.12	
3515.1	6.82	1.29	1.15	0.96	0.76	0.67	0.86		
a^3D-z^3D^o									
3446.3	6.70				1.18	0.78	0.67	0.92	
3472.5	6.24					0.98	0.74	1.29	
a^3D-z^3P^o									
3493.0	6.64					0.75	0.57	0.88	1.22
3524.5	6.95		0.97	0.84	0.59	0.45	0.63	1.24	

TABLE 2 (Cont'd)

El. Mult. λ	Log gf	Ce 4992 4994	4995 4996	4999 5000	5001 5002	5004	5006 5008	5010 5011	5014 5015	5071	5074	5078	5080	5083	5084	5085
Mg I																
3^3P^o-3^3D																
3829.4	9.79				0.98	0.95	0.76	0.53	0.48	0.56	0.91	1.38				
3832.3	10.13			1.38	0.77	0.72	0.66	0.48	0.35	0.52	0.84	1.29	1.36			
3838.3	10.32			0.73	0.61	0.56	0.45	0.37	0.25	0.37	0.55	0.90	1.17			
Al I																
3^2P^o-4^2S																
3944.0								0.96	0.76	1.14						
3961.5							1.08	0.84	0.69	0.90						
Cr I																
a^7S-y^7P^o																
3578.7	7.02				0.96	0.78	0.68	0.52	0.32	0.54	0.83	1.47				
3593.5	6.98				0.80	0.68	0.65	0.47	0.37	0.52	0.99	1.55				
3605.3	6.82				0.99		0.71	0.49	0.36	0.66	1.32					
Ti II																
b^4F-z^4F^o																
3318.0	1.18		1.03	0.84	0.92		0.52	0.43	0.37	0.53	0.61	0.92				
3322.9	2.05	0.40	0.38	0.30	0.39		0.37	0.27	0.20	0.31	0.35	0.36		0.79	1.11	
3326.8	1.09			0.82	0.72		0.49	0.48	0.42	0.47	0.63	0.84	1.06			
3329.5	1.86	0.51	0.52	0.32	0.44		0.34	0.31	0.24	0.34	0.30	0.45	0.84	0.88	1.42	
3335.2	1.75	0.66	0.52	0.40	0.50		0.45	0.49	0.30	0.36	0.41	0.54	0.73	0.97	1.27	
3340.3	1.62	0.60	0.50	0.41	0.49		0.38	0.32	0.25	0.38	0.41	0.58		1.05		
3343.8	1.06			1.01	0.97		0.60	0.53	0.45	0.58	0.70	1.19	1.19	1.19		
3346.7	1.17			0.85	0.67		0.53	0.53	0.42	0.49	0.66	0.98	1.05			
b^4P-z^4S^o																
3332.1	2.85			0.83	0.72		0.55	0.50	0.45	0.50	0.69	0.92	1.19			

TABLE 2 (Cont'd)

$a^2F\text{-}z^2G^o$																
3341.8	2.13	0.39	0.32	0.28	0.33		0.33	0.30	0.20				0.82	0.85	1.20	
$a^4F\text{-}z^4G^o$																
3361.2	2.00									0.45		0.50	0.55	0.64	0.73	1.14
3372.8	2.30	0.27	0.26	0.21	0.36			0.17		0.16	0.30	0.35	0.43	0.54	0.75	
3380.3	1.56	0.56	0.44	0.35	0.37		0.33	0.28	0.15	0.22	0.37	0.52	0.83	1.16	1.40	
3383.8	2.23	0.34	0.26	0.20	0.27		0.32	0.24	0.19			0.41	0.50	0.55	0.77	1.38
3387.8	1.68	0.46	0.46	0.36	0.36		0.34	0.30	0.21	0.26	0.39	0.38	0.58	0.90		
3394.6	1.67	0.64	0.53	0.44	0.46		0.42	0.38	0.29	0.27	0.43	0.47	0.59	0.95	1.52	
3407.2	0.43						0.76	0.58	0.47	0.55	0.97	1.22				
3409.8	0.39						0.98	0.67	0.51	0.64	1.13					
$b^4F\text{-}z^4G^o$																
3444.3	1.43	0.72	0.73	0.65	0.57		0.49	0.43	0.31	0.40	0.49	0.75	0.78	1.45		
3461.5	1.34	0.76	0.81	0.56	0.60	0.47	0.45	0.36	0.34	0.40	0.50	0.73	0.91			
3477.2	1.29			0.66	0.61	0.58	0.39	0.37	0.31	0.38	0.49	0.82	0.95			
3489.8	0.41					1.03	1.05	0.79	0.44	0.73	1.12	1.65				
3491.1	1.12			0.83	0.71	0.40	0.48	0.44	0.47	0.42	0.54	0.87	1.11			
3500.3	0.35					0.93	0.89	0.73	0.64	1.02	1.54					
$b^2G\text{-}y^2G^o$																
3504.9	3.43				0.64	0.72	0.69	0.58	0.54	0.61	0.76	1.03				
3510.8	3.35					0.72	0.82	0.74	0.55	0.64	0.85	1.33				
$a^2F\text{-}z^4D^o$																
3561.6	0.96						1.37	0.83	0.79	1.19						
3573.7	1.11				1.02	1.04	1.02	0.66	0.53	0.83	1.04	1.57				
3596.1	1.19		1.09	0.80	0.71	0.80	0.71	0.62	0.52	0.54	0.85	1.09				
$a^2P\text{-}z^2S^o$																
3624.8	2.20					0.80	0.68	0.58	0.58	0.82	1.00	1.02	1.23			
3641.3	2.35				0.73	0.69	0.64		0.55	0.83	1.18					
$a^2F\text{-}z^2D^o$																
3685.2	2.52	0.48	0.32	0.44	0.34	0.23	0.40	0.22	0.31	0.38	0.32	0.40	0.59	0.68	0.99	
$a^2F\text{-}z^2F^o$																
3759.3	2.48	0.41	0.35	0.34	0.27	0.22	0.36	0.28	0.35			0.37	0.43	0.59	0.98	
3761.3	2.36	0.50	0.40	0.36	0.28	0.30	0.34	0.28	0.31	0.19	0.33	0.39	0.46	0.67	0.95	1.38

TABLE 2 (Cont'd)

El. Mult. λ	Log gf	Ce 4992 4994	4995 4996	4999 5000	5001 5002	5004	5006 5008	5010 5011	5014 5015	5071	5074	5078	5080	5083	5084	5085
$a^2G-z^2G^o$																
3900.5	2.42				0.78	0.74	0.57	0.56	0.50	0.53	0.73	0.87	1.17			
3913.5	2.38				0.88	0.88	0.57	0.54	0.48	0.56	0.71	0.90	1.27			
Cr II																
$a^4D-y^4P^o$																
3336.4	10.00						0.63	0.57	0.49	0.60	0.84	1.13				
3339.8	10.14	0.99		0.70	0.77		0.53	0.51	0.48	0.45	0.64	0.90		1.11		
3342.6	10.23	0.90	1.04	0.74	0.64		0.47	0.48	0.48	0.57	0.60	0.77	1.16	1.33		
3347.8	10.05			0.97	0.84		0.69	0.61	0.46	0.60	0.74	0.96	1.05			
3358.5	10.32	0.56	0.68	0.53	0.61		0.48	0.41	0.34	0.39	0.57	0.56	0.70	0.92	1.54	
3368.1	10.63	0.43	0.47	0.39	0.43		0.41	0.33	0.29	0.38	0.37	0.44	0.59	0.50	0.76	1.14
$a^4D-z^4P^o$																
3382.7	10.10	0.73	0.87	0.79	0.66		0.57	0.51	0.45	0.50	0.61	0.84	0.94	1.20		
3391.4	9.64							0.93	0.78	0.77	1.07					
3403.4	10.27	0.75	0.71	0.61	0.55		0.49	0.49	0.43	0.47	0.51	0.59	0.67	0.96	1.39	
3408.8	10.40	0.63	0.54	0.46	0.49		0.45	0.45	0.39	0.44	0.48	0.55	0.60	0.89	1.00	
3421.2	10.27	0.81	0.76	0.73	0.71		0.59	0.55	0.40	0.48	0.58	0.71	0.82	1.22	1.31	
3422.8	10.32	0.56	0.54	0.45	0.53		0.45	0.40	0.39	0.34	0.38	0.47	0.61	0.70	0.92	
3433.3	10.30	0.71	0.61	0.55	0.63		0.46	0.39	0.33	0.44	0.57	0.64	0.72			
$a^4D-z^6P^o$																
3495.4	9.06								0.95	1.09	1.35					
3511.8	8.96						1.18		0.92	1.04	1.25					
Sc II																
$a^3D-z^3P^o$																
3369.0	7.16						0.78	0.52	0.40	0.62	1.06					
3372.2	7.28						0.49	0.48		0.48	0.66	0.96	1.11			1.14

TABLE 2 (Cont'd)

a^3D-z^3D^o													
3558.5	6.87			1.08	0.82	0.75	0.63	0.52	0.48	0.64	0.93	1.18	1.26
3567.7	6.78				1.09	0.85	0.74	0.69	0.63	0.71	0.94	1.54	
3572.5	7.21			1.02	0.61	0.57	0.56	0.51	0.42	0.43	0.65	1.01	1.12
3576.3	7.11				0.78	0.71	0.61	0.56	0.44	0.55	0.79	1.30	1.47
3580.9	7.31									0.59	0.94	1.46	
3590.5	6.58				1.22	1.19	0.99	0.73	0.62	0.75	1.27		
a^3D-z^3F^o													
3613.8	7.31			0.78	0.54	0.42	0.45	0.45	0.39	0.47	0.59	0.89	0.95
3630.7	7.18			0.79	0.64	0.61	0.49	0.44	0.31	0.57	0.73	1.27	1.42
3642.8	7.10			0.61	0.56	0.65	0.52	0.40	0.37	0.49	0.73	1.14	1.08
3645.3	6.59				0.92	0.83	0.82	0.53	0.58	0.68	1.02		
3651.8	6.66				0.92	1.05	0.84	0.67	0.63	0.73	1.07		
Mn II													
a^5D-z^5P^o													
3442.0	9.70	0.66	0.55	0.44	0.50		0.42	0.40	0.31	0.33	0.40	0.52	0.60	1.00
3460.3	9.55	0.79	0.74	0.54	0.59		0.41	0.39	0.38	0.37	0.51	0.74	0.81	
3482.9	9.35			0.79	0.78	0.54	0.58	0.58	0.43	0.48	0.56	0.92	0.99	
3488.7	9.28			0.85	0.83	0.61	0.58	0.59	0.57	0.46	0.66	0.91	0.93	
3495.8	8.85					0.77	0.60	0.61	0.48	0.54	0.80	1.23	1.36	
3496.8	8.42						1.02	0.84	0.62	0.95				
3497.5	8.78					0.76	0.79	0.64	0.61	0.60	1.18			
V II													
a^3F-z^5D^o													
3517.3	7.78						0.96	0.89	0.80	0.93	1.24		
a^3F-y^3D^o													
3530.8	7.68						1.06	0.93	0.84	1.06			
3545.2	7.85						1.12	0.97	0.88	0.88	1.32		
3556.8	8.10			1.15	0.88	0.81	0.74	0.58	0.55	0.65	0.95	1.11	1.29	
Fe II													
a^4D-z^6D^o													
3255.9		0.88	0.57	0.47	0.50	0.46		0.37	0.31	0.36	0.48	0.57		0.81
3277.3		0.88	0.55	0.59	0.66			0.38	0.45	0.34	0.45	0.53		0.97

TABLE 2 (Cont'd)

El. Mult. λ	Log gf	Ce 4992 4994	4995 4996	4999 5000	5001 5002	5004	5006 5008	5010 5011	5014 5015	5071	5074	5078	5080	5083	5084	5085
3281.3		1.20	0.88	0.62	0.65	0.54		0.45	0.51	0.43	0.62	0.93		1.46		
3295.8		1.33	1.06	0.95	0.93	0.74	0.75	0.59	0.48	0.51	0.82	1.15			1.45	
3303.5			1.73		1.29	1.02	0.86	0.68	0.53	0.72	1.13	1.33				
3314.0				1.87		1.48	1.49	0.99	0.81	1.08						
$a^4P\text{-}z^4D^o$																
3166.7					1.02		0.96	0.90		0.76	1.53					
3170.3				1.00	0.91		0.64	0.76		0.62	0.94					
3186.7			0.49	0.38	0.40		0.40	0.38		0.31	0.40	0.53		1.02	1.01	
3192.9			0.66	0.55	0.57		0.45	0.45		0.32	0.53	0.77		0.87		
3193.8			0.55	0.42	0.48		0.51	0.45		0.38	0.53	0.58		0.83	1.12	
3210.4		0.55	0.40	0.26	0.39		0.35	0.40	0.19	0.30	0.42	0.39		0.78	1.09	
3213.3		0.31	0.36	0.25	0.35		0.34	0.32	0.30	0.24	0.33	0.42		0.48	0.73	0.84
$a^4P\text{-}z^4F^o$																
3183.1			0.69	0.56	0.55		0.41	0.43		0.40	0.58	0.60				
3185.3				1.17	1.09		0.78	0.65		0.60	0.98	1.12				
3196.1			0.65	0.52	0.46		0.37	0.44		0.36	0.55	0.66		0.85	1.42	
$b^4D\text{-}y^4F^o$																
3247.2								0.76	0.62							
$b^4D\text{-}x^4D^o$																
3177.5			1.30	0.99	1.13		0.93	0.73								
$c^2G\text{-}z^2F^o$																
3243.7				1.14	1.14			1.01	1.09							
3247.4								0.80	0.61							
$c^2D\text{-}y^2F^o$																
3179.5			1.08	0.96	0.99		0.93	0.58								

TABLE 3*

LOG W AND LOG N FOR *Ca* I, *Ca* II, AND H, 1947–1948

Line	4992, 94 46.1	4995, 96 40.4	4999, 00 32.0	5001, 02 25.8	5004 24.3	5006, 08 17.6	5010, 11 11.6	5014, 15 9.4	5071 11.5	5074 18.2	5078 25.5	5080 27.6	5083 41.5	5084 48.0
Ca II, K...	− 0.03 15.3	− 0.03 15.3	0.00 15.5	0.02 16.1	0.04 16.3	0.01 16.4	0.33† 17.3	0.46† 17.6	− 0.11 15.7	− 0.12 15.6	− 0.16 14.7	− 0.28 13.8	− 0.30 13.4	− 0.43 13.0
Ca I, 4227..	....	....	....	− 0.73 12.3	....	− 0.49 13.4	− 0.28 14.9	....	− 0.33 14.3	− 0.70 12.6	....	....	....	....
*H*7.....	− 0.31 15.6	− 0.25 15.9	− 0.24 16.0	− 0.25 15.9	− 0.24 16.0	− 0.24 16.0	− 0.21 16.2	− 0.32 15.5	− 0.35 15.4	− 0.32 15.5	− 0.33 15.4	− 0.35 15.4	− 0.47 14.9	− 0.71 14.1
*H*8.....	− 0.33 15.6	− 0.33 15.6	− 0.27 15.9	− 0.23 16.2	− 0.27 15.9	− 0.20 16.4	− 0.33 15.6	− 0.19 16.5	− 0.23 16.2	− 0.32 15.7	− 0.32 15.7	− 0.41 15.4	− 0.54 14.9	− 0.65 14.7
*H*9.....	− 0.40 15.6	− 0.40 15.6	− 0.38 15.7	− 0.32 15.9	− 0.27 16.1	− 0.34 15.8	− 0.28 16.1	− 0.38 15.7	− 0.38 15.7	− 0.41 15.6	− 0.40 15.6	− 0.46 15.4	− 0.78 14.6	− 1.04 14.2
*H*10.....	− 0.44 15.5	− 0.38 15.8	− 0.30 16.1	− 0.28 16.2	− 0.28 16.2	− 0.24 16.5	− 0.27 16.2	− 0.25 16.4	− 0.26 16.3	− 0.31 16.1	− 0.41 15.7	− 0.44 15.6	− 0.69 14.9	− 1.04 14.3
*H*11.....	− 0.50 15.5	− 0.51 15.4	− 0.47 15.5	− 0.46 15.5	− 0.37 15.9	− 0.36 15.9	− 0.32 16.1	− 0.29 16.2	− 0.38 15.9	− 0.41 15.8	− 0.53 15.3	− 0.63 15.1	− 0.70 14.9	− 1.03 14.5
*H*12.....	− 0.55 15.5	− 0.45 15.8	− 0.50 15.6	− 0.44 15.8	− 0.45 15.8	− 0.41 15.9	− 0.41 15.7	− 0.39 16.0	− 0.39 16.0	− 0.41 16.0	− 0.53 15.5	− 0.63 15.3	....	....

* Column headings are plate number, followed by heights in units of 10^6 km. Entries in table for each line are, above, log W in angstroms; below, log N. Entries marked † have been corrected for the effect of K-star line.

Curves of growth were constructed from the measured equivalent widths of the metallic lines as before, by plotting log $(w \times [3700/\lambda])$ against log $(gf \times [\lambda/3700])$, where w is the equivalent width in angstroms and g is the weight factor; and they were compared with curves calculated from the theoretical formulae. As far as possible, separate curves of growth were constructed at each atmospheric height for the lines of common excitation potential of each ion. For both *Fe* I and *Ti* II the measured lines covered a sufficient range of excitation potential to permit derivation of excitation temperatures.

IV. RESULTS

a) EVALUATION OF DOPPLER WIDTHS FROM CURVES OF GROWTH

For the 1939–1940 eclipse, neutral and ionized lines were plotted together in forming the observed curves of growth, and an increase of Doppler width with height was found.[2] Since neutral and ionized lines were plotted separately for the 1947–1948 eclipse, Doppler widths were estimated for both types of lines, as far as possible at each height. These estimates, obtained by fitting the observations to theoretical curves, were made independently by both authors, and in only two instances did they differ by more than

TABLE 4

LOG N AS FUNCTION OF HEIGHT FOR *H*, *Ca* I, *Ca* II
(Revised Values for 1939–1940 Eclipse)

Atom	Height $\times 10^{-6}$ Km								
	6.9	8.4*	14.3	15.3*	20.8	23.3*	28.0	30.7*	38.0*
H	15.5	15.8	15.6	15.9	15.3	15.7	15.2	15.4	15.6
Ca I	17.4	17.1	13.6	12.7	11.9	.....	.....	.....	.....
Ca II	18.6	18.0	16.4	16.2	15.5	15.9	14.5	14.4	14.0

* Egress.

0.02 A. Mean results are given in Table 5, together with corresponding turbulent velocities V_T and the data from the 1939–1940 eclipse on the revised height scale.

It is to be noted that the marked increase of $\Delta\lambda_D$ with height derived from the 1939–1940 data is not confirmed by the more recent material. Although there appears to be a slight tendency for the turbulent velocities of the ionized lines to increase upward, the most striking feature of Table 5 is the appearance of a systematic difference between the turbulent velocities for neutral and for ionized particles (Fig. 1). We can think of no observational deficiency to account for this difference, which, although small, appears so consistently that we are strongly inclined to believe in its reality. In fact, a difference of this kind between the neutral and ionized particle velocities is capable of accounting for the apparent rise of V_T with height, found in 1939–1940, for the following reason. The determination of $\Delta\lambda_D$ at this eclipse depended mostly upon the neutral lines at the lower heights and chiefly upon the ionized lines at the higher levels; hence an apparent increase of $\Delta\lambda_D$ with height is just what one would expect if the true situation is as given in Table 5. We feel that this consideration removes the inconsistency between the results for the two eclipses.

The explanation of the difference between the values of ionized and neutral $\Delta\lambda_D$ must be something like this: a ray through the chromosphere of Zeta Aurigae must penetrate regions of higher- and of lower-than-average ionization, and the mass motions in the regions of higher ionization must tend to be somewhat greater than in those of lower

ionization. A further important point contained in Table 5 is that there is no evidence for differences in turbulent velocity between ingress and egress.

Curves of growth were constructed also for the hydrogen lines from $H7$ to $H12$ for heights up to 48×10^6 km. All these curves yielded estimated values of $\Delta\lambda_D$ of approximately 0.14–0.16 A, with no evidence for a systematic variation with height. The expression for $\Delta\lambda_D$, including both thermal and mass motions, is

$$\Delta\lambda_D = \frac{\lambda}{c}\left(\frac{2kT}{m} + V_T^2\right)^{1/2}. \tag{1}$$

TABLE 5

DOPPLER WIDTHS AND TURBULENT VELOCITIES

1947–1948 ECLIPSE

Height (10^6 Km)	$\Delta\lambda_D$ (A)		V_T (Km/Sec)	
	Neut.	Ion.	Neut.	Ion.
9.4.....	0.10	0.13	8.1	10.5
11.5*.....	.10	.14	8.1	11.4
11.6.....	.10	.12	8.1	9.7
17.6.....	.09	.13	7.3	10.5
18.2*.....	.10	.14	8.1	11.4
24.3.....	0.10	.16	8.1	13.0
25.5*.....	.....	.15	.....	12.2
25.8.....	.....	.14	.....	11.4
27.6*.....	.....	.16	.....	13.0
32.0.....	.....	$\geq$ .16	.....	$\geq$13.0
40.4.....	.....	$\geq$ .16	.....	$\geq$13.0
41.5*.....	.....	$\geq$ .16	.....	$\geq$13.0
46.1.....	.....	$\geq$ .16	.....	$\geq$13.0
48.0*.....	.....	$\geq$0.16	.....	$\geq$13.0

* Egress.

1939–1940 ECLIPSE

Height (10^6 Km)	$\Delta\lambda_D$ (A) Neut.+Ion.	V_T (Km/Sec) Neut.+Ion.
6.9.....	0.08	6.4
8.4*.....	.08	6.4
14.3.....	.10	8.0
15.3*.....	.13	10.4
20.8.....	.13	10.4
23.3*.....	.15	12.1
28.0.....	0.16	12.9

* Egress.

For hydrogen at 4000° the first term alone yields a value $\Delta\lambda_D = 0.10$ A. If, in addition, there are mass motions corresponding to those given in Table 5 for the neutral particles, i.e., about 8 km/sec, the resulting combined $\Delta\lambda_D$ is 0.14 A. The observed $\Delta\lambda_D$ for hydrogen is therefore at least roughly consistent with the excitation temperatures and turbulent velocities deduced for the metals.

b) DOPPLER WIDTHS DURING TOTALITY

The mass motions derived from observations of the chromospheric lines are necessarily those motions approximately perpendicular to a line from the center of the star, and it would be of considerable interest to know how these motions compare with those in a radial direction. The radial motions can be obtained from direct observations of the star but will correspond to a considerably lower atmospheric level than do the transverse motions.

Several spectrograms of Zeta Aurigae were taken during totality with the 114-inch camera for the purpose of deriving the turbulent velocity in the reversing layer. The yellow-green region (dispersion 5.6 A/mm) was selected in order to minimize the effects of blends. Owing to instrumental difficulties, only one of these plates (Ce 5028) was satisfactory for the purpose. Equivalent widths of about sixty lines were measured in multiplets of *Fe* I, *Ti* I, *V* I, and *Ca* I in which the relative *f*-values are known from

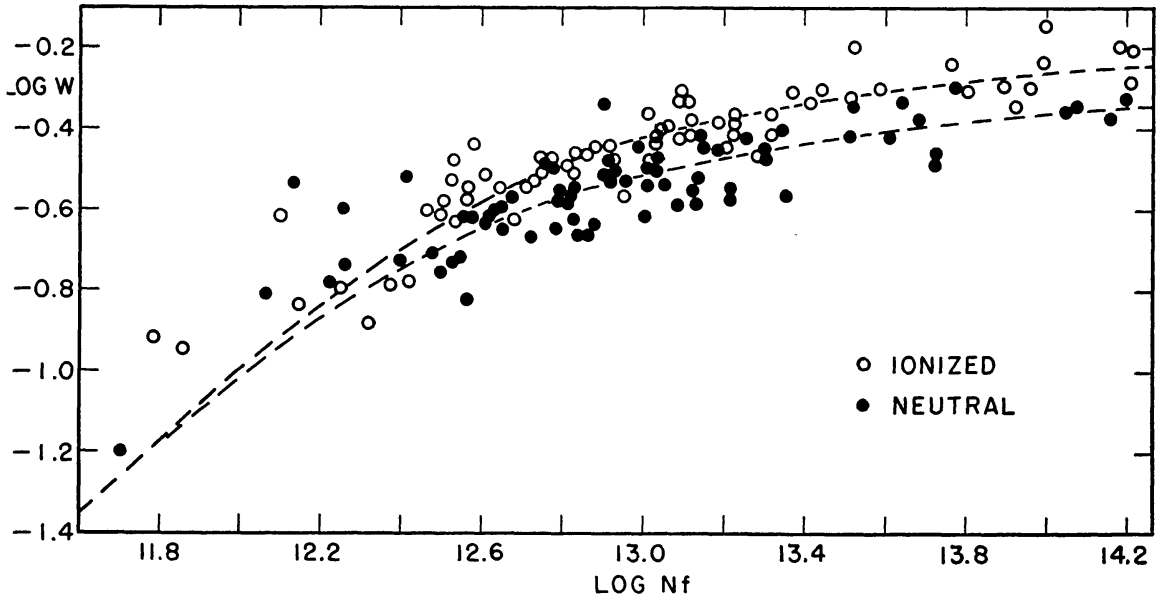

FIG. 1.—Curves of growth at height 9.4×10^6 km during ingress. The theoretical curves are for $\Delta\lambda_D$ = 0.13 A (*upper*) and 0.10 A (*lower*).

laboratory data. The intensities were combined into a curve of growth in the usual way and yielded a $\Delta\lambda_D$ of 0.05 A, corresponding to V_T = 2.3 km/sec.

Unfortunately, the variation of V_T with height given in Table 5 is so uncertain (for the neutral lines there is no variation) that we do not believe it possible to extrapolate downward to the level of normal line formation. Apparently, judging from the results for the ionized lines, there is a tendency for V_T to increase slightly upward, and to this extent the disk lines and the chromospheric lines yield Doppler widths which differ in the correct sense. A numerical comparison, however, appears to lie beyond the proper use of the existing data, and we are unable to say whether the transverse and radial components of the mass motions are the same at a given height or not.

c) EXCITATION TEMPERATURES

Excitation temperatures have been determined both for *Fe* I and for *Ti* II, and the results are given in Table 6 and in Figure 2. The a^5 F and a^3 F states of *Fe* I, with excitation potentials of 0.86 and 1.48 volts, respectively, were compared with the ground state, a^5 D, and gave fairly accordant results. For *Ti* II only the a^2 F state at 0.57 volts

E.P. was far enough from the ground state, a^4F, and produced enough lines to yield reasonably good values.

In Figure 2 the *Fe* I excitation temperatures as determined at the 1939–1940 eclipse are included for comparison, and the agreement with the 1947–1948 values is fair. Taking all the data into account, there seems little doubt that T_{ex} does increase with height and at about the same rate as was indicated by the 1939–1940 data. Also, considering the scatter of the individual points, there are no certain differences in T_{ex} between ingress and egress.

From the plate (Ce 5028) taken during totality, a well-determined excitation temperature of 2880° was found from the lines of *V* I. This value is probably a little lower than the effective temperature of the star, which is generally considered to be about 3200°.[8]

TABLE 6

CHROMOSPHERIC EXCITATION TEMPERATURES IN ZETA AURIGAE

Height (10^6 Km)	*Fe* I			*Ti* II
	a^5F	a^3F	Mean	a^2F
9.4.....	4110	4540	4325	2790
11.5*.....	4200	5060	4630	2660
11.6.....	4380	4620	4500	3780
17.6.....	4290	4340	4315	3780
18.2*.....	4600	4750	4675	4950
24.3.....	5100	4930	5015	3800
25.5*.....	.....	.....	.....	4950
25.8.....	.....	.....	.....	7750
27.6*.....	.....	.....	.....	5410
32.0.....	.....	.....	.....	5410
41.5*.....	.....	.....	.....	7360
48.0*.....	.....	.....	.....	6520

* Egress.

d) NUMBERS OF ATOMS IN LINE OF SIGHT AND APPARENT GRADIENTS

The effective numbers of atoms in the line of sight at various heights were read for certain lines from the curves of growth. This material is given in Table 7, where corrections to the ground state by means of appropriate Boltzmann factors are included. Excitation temperatures for the corrections were read from the straight line of Figure 2. To get the numbers of atoms responsible for producing the lines listed in Table 7, it is necessary only to divide the entries by the *f*-values.

Mean values of apparent gradients, $\Delta \log N/\Delta h$, calculated from the values of $\log N$ show a large scatter, as is to be expected, since the derived values of $\log N$ do not form a smooth, monotonic progression. Data of this type are best shown graphically.

Figures 3, 4, and 5 show $\log N$ plotted against height for *Ca* I, *Ca* II, and *H* (first excited state) for both eclipses. Note that in all three diagrams ingress and egress of 1939–1940 agree approximately with egress 1947–1948, but that ingress 1947–1948 stands off in the direction of lower gradient and larger $\log N$ values.[9] Note also that for each particle all four sets of data show a strong tendency to converge to very similar

[8] P. Wellmann, *Mitt. Hamburger Sternwarte, Bergedorf*, No. 76, 1951.

[9] H. L. Welsh, *J.R.A.S. Canada*, **43**, 217, 1949, finds a similar result for *Ca* II alone.

values of log N at the lowest observed heights. Much the same behavior is exhibited by all the metallic lines. Typical of these are the curves for *Fe* I and *Mn* II shown in Figure 6.

In Figure 7 are shown the mean log Nf versus height–curves for ionized and neutral metals for the 1947–1948 eclipse. Two sets of curves have been drawn for the ions, one for low-excitation lines, the other for lines of higher excitation, since the shape of the curve seems to depend somewhat upon the degree of excitation. It is not certain, however, whether this difference is real, since in all these data the Boltzmann correction factors to the ground state are included and, as more highly excited levels are more sensitive to errors in Boltzmann corrections, the differences between the two curves for the ions might be attributable to this source.

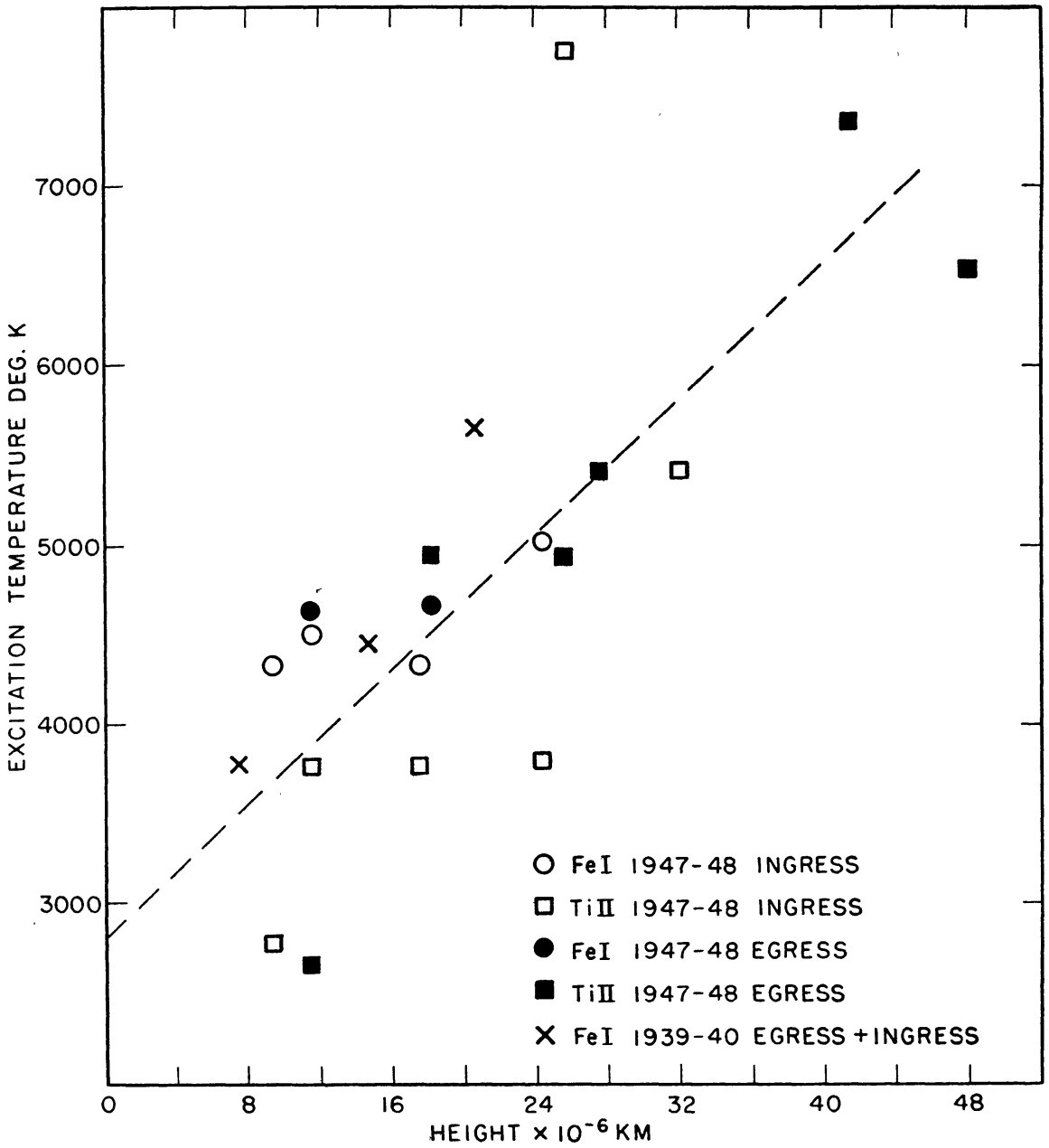

FIG. 2.—Dependence of excitation temperature on height

TABLE 7

VALUES OF LOG *Nf* CORRECTED TO GROUND STATE BY BOLTZMANN FACTOR

ATOMIC STATE	λ	E.P.	HEIGHT × 10^{-6} KM													
			9.4	11.5*	11.6	17.6	18.2*	24.3	25.5*	25.8	27.6*	32.0	40.4	41.5*	46.1	48.0*
Fe I a^5D...	(3719.9)	0.00	13.77	13.22	13.42	12.94	12.39	12.58	12.05	12.36	11.75	.....	.....	.....	.....	.....
Fe I a^5F....	(3709.2)	0.86	13.96	13.40	13.60	12.95	12.47	12.62	11.86	12.49	11.78	.....	.....	.....	.....	.....
Fe I a^3F....	(3815.8)	1.48	15.17	14.72	14.74	14.24	13.47	13.54	13.23	13.40	.....	.....	.....	.....	.....	.....
Ni I a^3D...	(3414.8)	0.02	12.95	12.25	12.60	12.13	11.26	11.90	.....	11.75	.....	.....	.....	.....	.....	.....
Mg I 3^3P....	(3829.4)	2.70	17.40	16.45	16.48	15.41	15.03	14.74	13.98	14.57	13.72	.....	.....	.....	.....	.....
Cr I a^7S....	(3578.7)	0.00	14.20	12.87	13.19	12.61	12.04	12.38	11.44	12.20	.....	.....	.....	.....	.....	.....
Ti II a^4F....	(3387.8)	0.00	14.11	13.89	13.75	13.34	13.18	.....	12.81	12.99	12.34	12.92	12.70	12.01	12.55	11.62
Ti II b^4F....	(3318.0)	0.11	13.46	12.98	13.03	12.85	12.70	12.83	12.23	12.43	12.02	12.35	12.09	11.49	12.02	11.02
Ti II a^2F....	(3761.3)	0.57	14.58	14.30	14.46	13.95	13.97	13.91	13.51	13.98	13.07	13.64	13.43	12.74	13.14	12.32
Cr II a^4D...	(3336.4)	2.41	16.06	15.77	15.70	15.22	15.04	.....	14.46	14.57	14.25	14.25	13.86	13.40	13.67	12.92
Sc II a^3D...	(3369.0)	0.00	13.04	12.77	12.83	12.66	12.37	12.48	11.86	12.47	11.77	12.16	.....	.....	.....	.....
Mn II a^5D...	(3442.0)	1.77	15.79	15.70	15.56	15.16	14.92	14.75	14.22	14.39	14.09	14.18	13.90	13.30	13.62	.....
V II a^3F....	(3517.3)	1.07	13.66	13.53	13.54	13.17	12.89	12.95	12.57	12.85	12.34	12.51	.....	.....	.....	.....

* Egress.

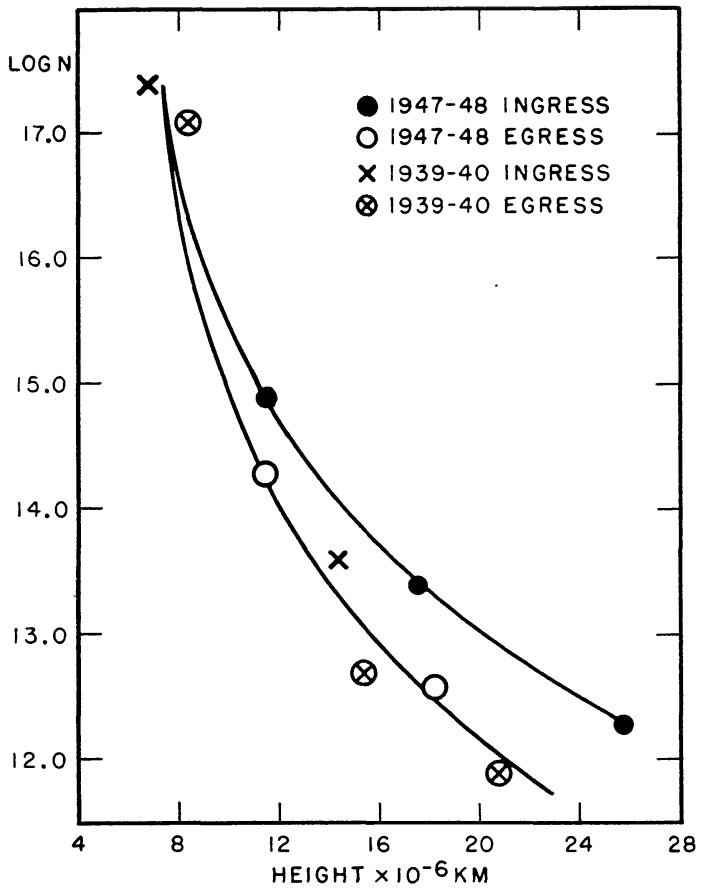

FIG. 3.—Log N versus height for *Ca* I

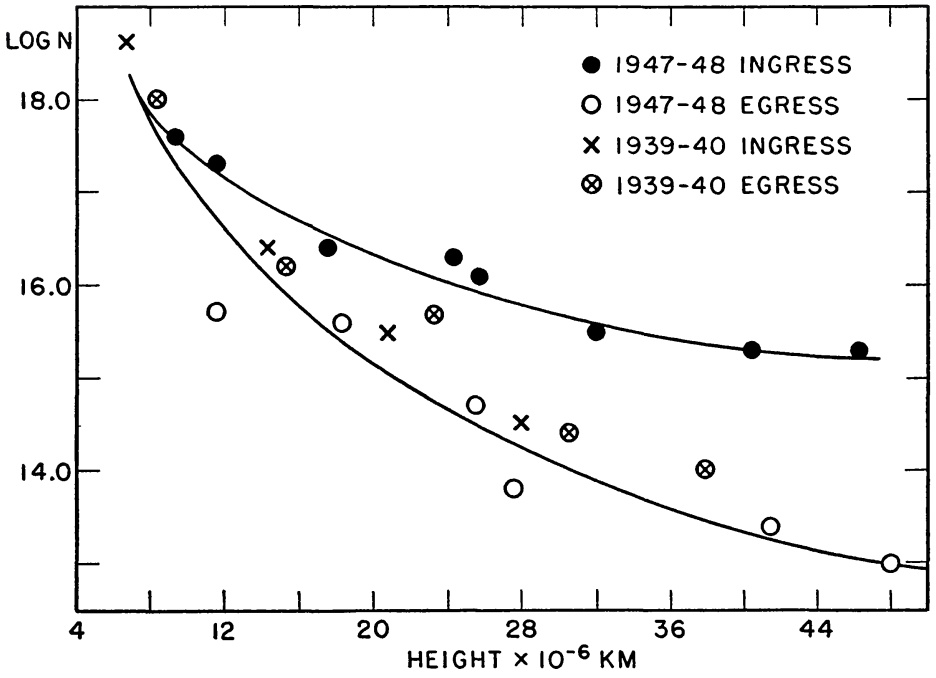

FIG. 4.—Log N versus height for *Ca* II

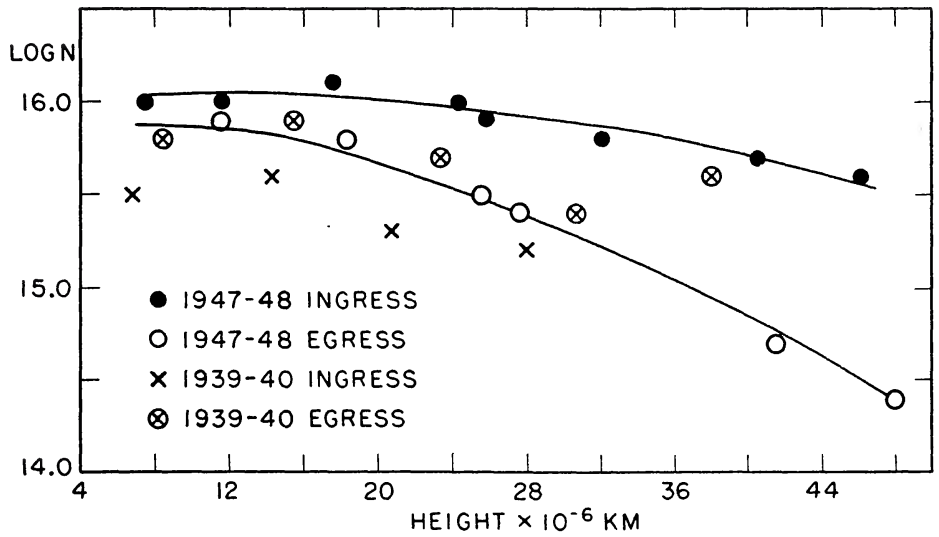

FIG. 5.—Log N versus height for first excited state of hydrogen

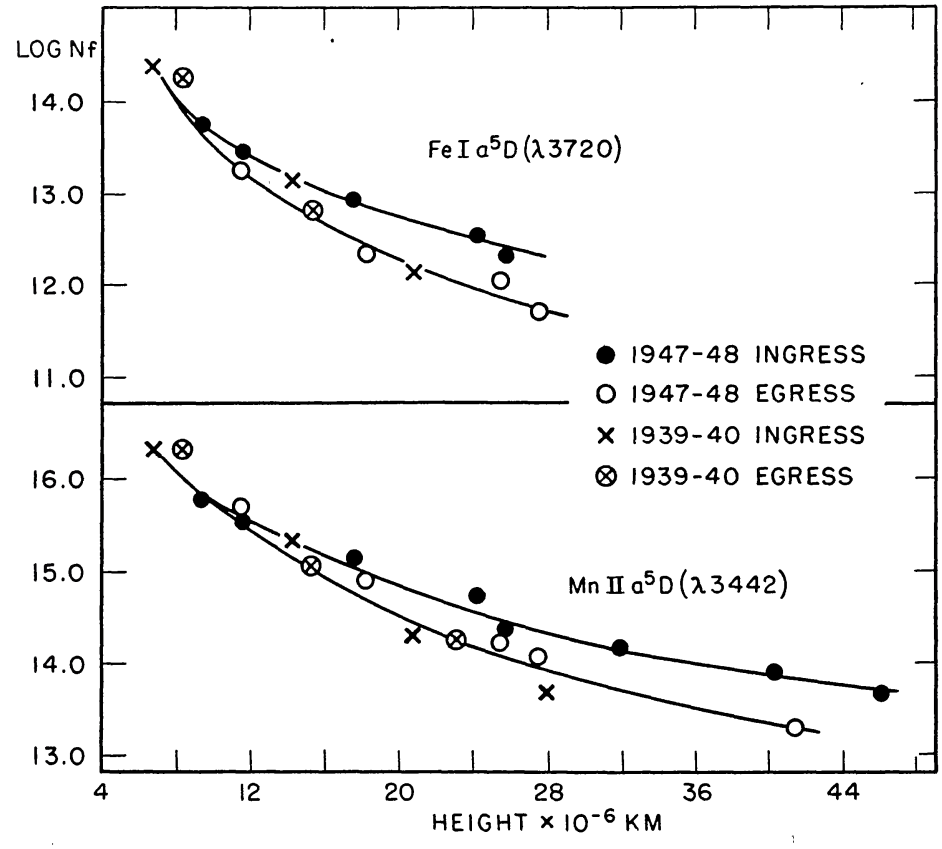

FIG. 6.—Log N versus height for *Fe* I and *Mn* II

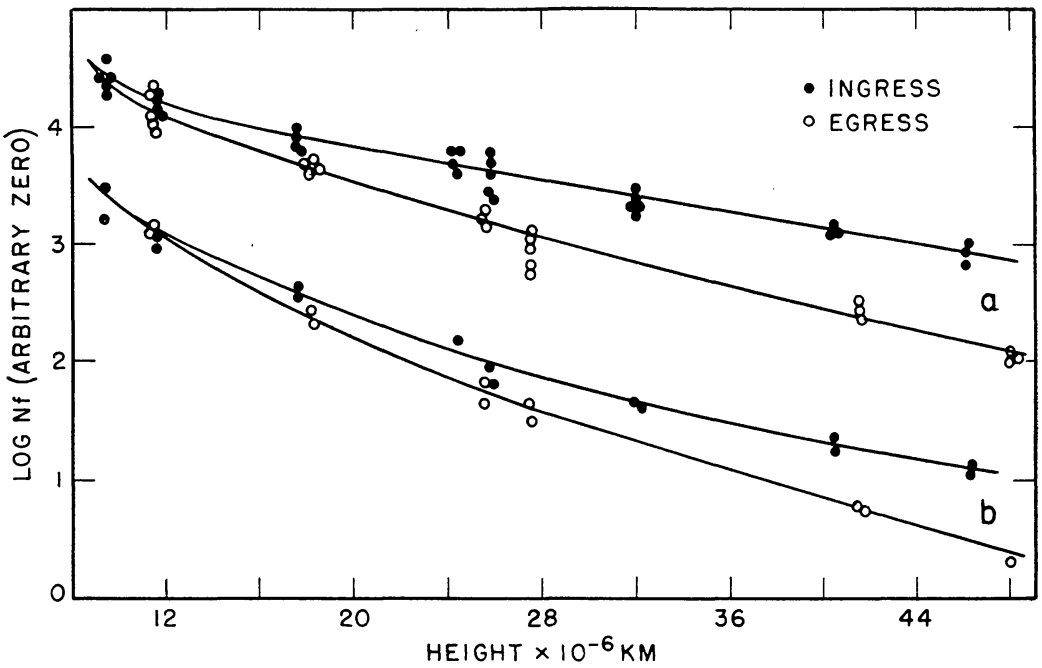

FIG. 7*a*.—Log *Nf* versus height for ionized metals, 1947–1948 eclipse. Curve *a*: *Ti* II, *Sc* II, *V* II; Curve *b*: *Cr* II and *Mn* II.

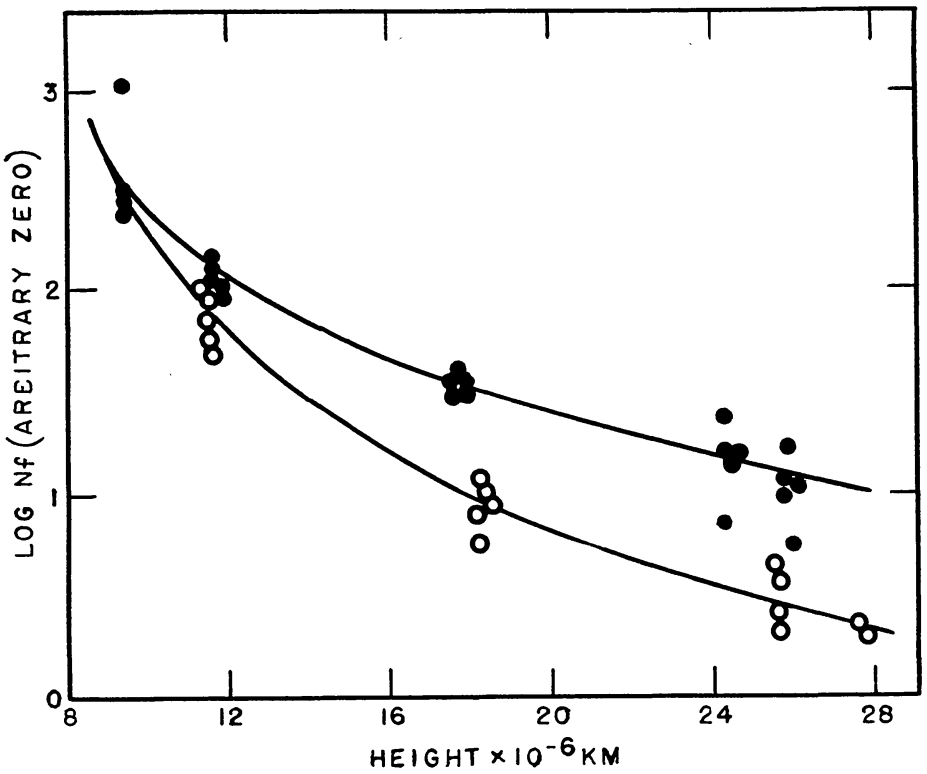

FIG. 7*b*.—Log *Nf* versus height for neutral metals, 1947–1948. Mean curves for *Fe* I, *Ni* I, *Cr* I

Values of log N for two stages of ionization of an element have hitherto been available only for calcium, and the *Ca* I and *Ca* II apparent gradients were found to be quite different in the earlier results.[2] This difference is confirmed by the more recent observations and is clearly evident by comparing Figures 3 and 4. Taking the ratio of $N(Ca\ \text{II})$ to $N(Ca\ \text{I})$ as a measure of the mean ionization of calcium along a ray, the very different apparent gradients for *Ca* I and *Ca* II indicate that the mean ionization of calcium varies rapidly with the height in the lower chromosphere. On the other hand, the approximate parallelism of the curves for other metallic ions and atoms does not show evidence of

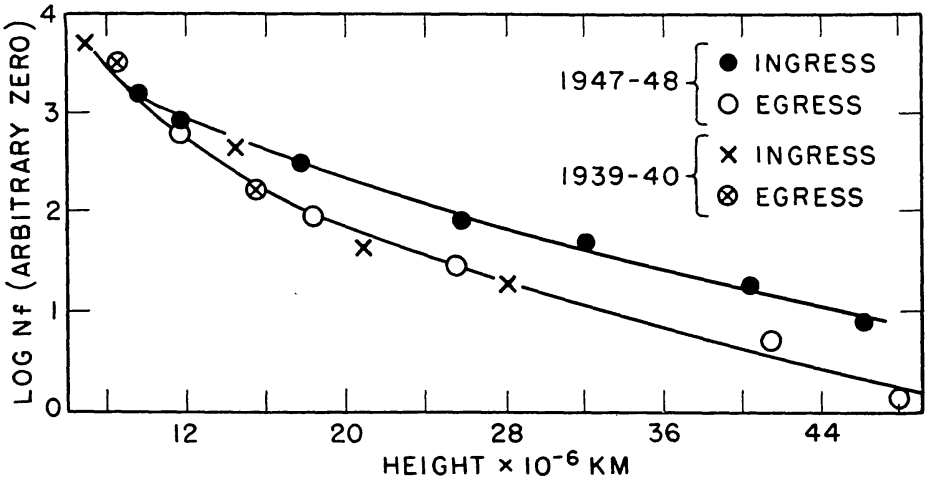

FIG. 8.—Log Nf versus height for *Fe* II

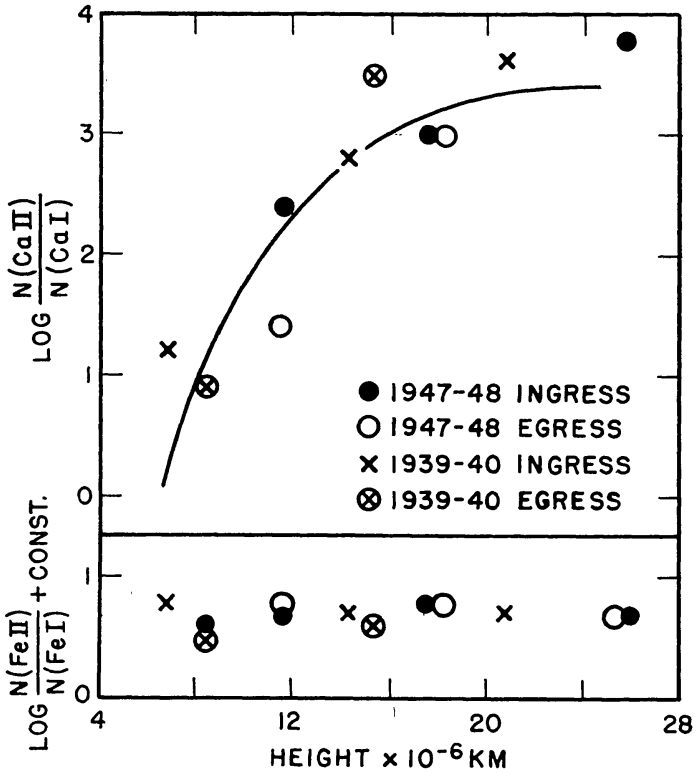

FIG. 9.—Mean ionization of *Ca* and *Fe* as function of height

much change in ionization with height, even though the atoms and ions compared are of different species.

Iron is the only element with enough lines in the spectrum from both the neutral and the singly ionized stage to permit a further study of mean ionization as a function of height. Intensities of about twenty-four lines of *Fe* II were measured on as many plates of both eclipses as possible. Unfortunately, no *f*-values are available for these lines, all of which lie in the region λλ 3167–3314, but they may be used to determine the rate of change with height of log N for *Fe* II. To do this, the log N for each line is read from the appropriate curve of growth. Then the values of Δ log N for each line are obtained between successive heights, and the means of these quantities, corrected differentially for temperature differences, should represent fairly well the rate of change of log N with height for *Fe* II. The dependence of log N upon height for *Fe* II derived in this fashion is shown in Figure 8. Finally, comparison of these results with those for *Fe* I yields the height dependence of log $[N(Fe\,\text{II})/N(Fe\,\text{I})]$, apart from an additive, indeterminate, constant.

e) MEAN IONIZATION AS FUNCTION OF HEIGHT

The mean ionizations of *Ca* and of *Fe* as functions of height are shown in Figure 9. Such a gross difference in behavior can hardly be accounted for by errors of any kind and must be considered real. Since the apparent gradients of *Fe* I and *Fe* II are quite similar to those of the other metallic atoms and ions (apart from calcium), the proper conclusion would seem to be this: the mean ionization of the metals is not a function of height over a range in which the total number of atoms in the line of sight decreases by a factor of about 100. Calcium presents an outstanding exception to this rule, showing an increase in N(ion.)/N(neut.) of more than 10^3 over the same range in height. It is noteworthy that in Figure 9 the ionizations of both calcium and iron during ingress 1947–1948 agree with those of the other atmospheric transits represented.

f) RADIAL VELOCITIES

Apart from studies of line intensity, measures of radial velocity of the chromospheric lines offer another line of attack on the problem of atmospheric structure. Most of the spectrograms used for photometric purposes at both eclipses have now been measured for radial velocity. Particularly for plates of the 1947–1948 eclipse, a special effort was made to answer two questions: First, are there, among the metallic lines (apart from *Ca* II), real differences in velocity between groups of strong lines as compared to groups of weak lines? Second, are there differences between lines of ions and of neutral atoms? Careful measurement of sizable groups of lines of the various kinds has shown that the answer to both questions is negative. Accordingly, all velocities of metallic lines, regardless of line strength and source of origin, have been lumped together in forming the mean values labeled "metals" in Table 8 and in Figures 10 and 11.

For the metallic lines the probable errors of the velocities are always considerably less than 1 km/sec. Except at the highest levels, these velocities depend upon measures of twenty or more selected lines. About eight hydrogen lines were measured on most plates, and for these also the probable errors are generally less than 1 km/sec. Since but two lines of *Ca* II are present, only an estimate of the accuracy may be made. On most plates the velocities of H and K agree to within about 2 km/sec, which may therefore be taken as a generous estimate of the probable error of the tabulated *Ca* II velocities. Hence we may conclude that all but the smallest differences shown in Figures 10 and 11 for the metals and for hydrogen almost certainly represent real velocity differences, while differences in *Ca* II velocity of as much as 3 or 4 km/sec are also probably real. At the highest observed levels, naturally, the number of available metallic lines falls off, and the probable error increases slightly.

With these estimates of accuracy in mind, some features of Figures 10 and 11 may be considered. The lines marked "Orbit" are calculated from Harper's elements[5] with the revised period of 972.16 days. The few measures in or close to totality fit the predicted velocity-curve fairly well, and there are not enough of them to show whether Harper's elements require further revision. The vertical lines marked "Eclipse" indicate the extent of the partial phases of the photometric eclipse.

TABLE 8

RADIAL VELOCITIES OF ZETA AURIGAE (KM/SEC)

1947–1948 ECLIPSE

Plates	JD 2432000+	Metals	*H*	*Ca* II
4992, 4994....	528.89	+11.9	+16.8	+11.8
4995, 4996....	529.68	16.0	16.7	14.9
4999, 5000....	530.84	17.0	17.9	15.8
5001, 5002....	531.70	14.2	13.3	18.1
5006, 5008....	532.83	18.8	19.1	23.7
5010, 5011....	533.67	18.8	16.1	25.6
5014, 5015....	533.96	16.7	16.9	19.3
5019*.....	535.69	15.2	.....	.....
5026*.....	542.71	17.9	.....	.....
5059*.....	571.60	23.8	.....	.....
5071.....	573.66	21.4	21.5	22.8
5074.....	574.58	21.5	21.0	19.0
5078.....	575.59	21.0	21.2	20.2
5080.....	575.88	17.8	19.3	18.0
5083.....	577.80	17.1	17.0	14.9
5084.....	578.71	20.4	18.6	17.4
5085.....	579.58	22.4	.....	20.3

*Totality.

1939–1940 ECLIPSE

Plates	JD 2429000+	Metals	*H*	*Ca* II
2183.....	614.82	+17.7	+15.5	+13.1
2188.....	615.82	14.1	17.1	12.1
2194.....	616.72	16.8	19.6	14.6
2202*.....	617.87	16.0	.....	.....
2205*.....	618.78	17.1	.....	.....
2243*.....	655.74	26.5	.....	.....
2245.....	656.66	24.8	.....	27.3
2248.....	657.62	26.1	26.3	28.4
2253.....	658.73	23.1	23.9	26.7
2254.....	659.74	22.4	18.9	21.8
2255.....	660.76	17.5	14.8	18.9

*Totality.

At both ingress and egress the general trend of the velocities is in the direction of a large deviation from the orbit immediately outside eclipse, followed by a return to, or at least toward, the orbital values. These deviations, therefore, cannot be due primarily to a rotation effect, although they are in the right sense if the star rotates in the direction of its orbital motion. Rather, they must be due to some kind of equatorial atmospheric current which exists in the lower chromospheric levels. This hypothetical current is by

no means constant, however. Note, for example, in Figure 10 the low *Ca* II velocities immediately preceding eclipse in 1939 as compared to the extremely high ones of about the same phase in 1947.[10] Another inconsistency is found in comparing the phases of maximum deviation at ingress with those at egress. At ingress the maximum deviations occur within about 1 day of first contact, while more than 4 days elapse after fourth contact before the maximum velocity deviations occur at egress. Moreover, except for *Ca* II, the egress deviations are about twice as large as those at ingress.

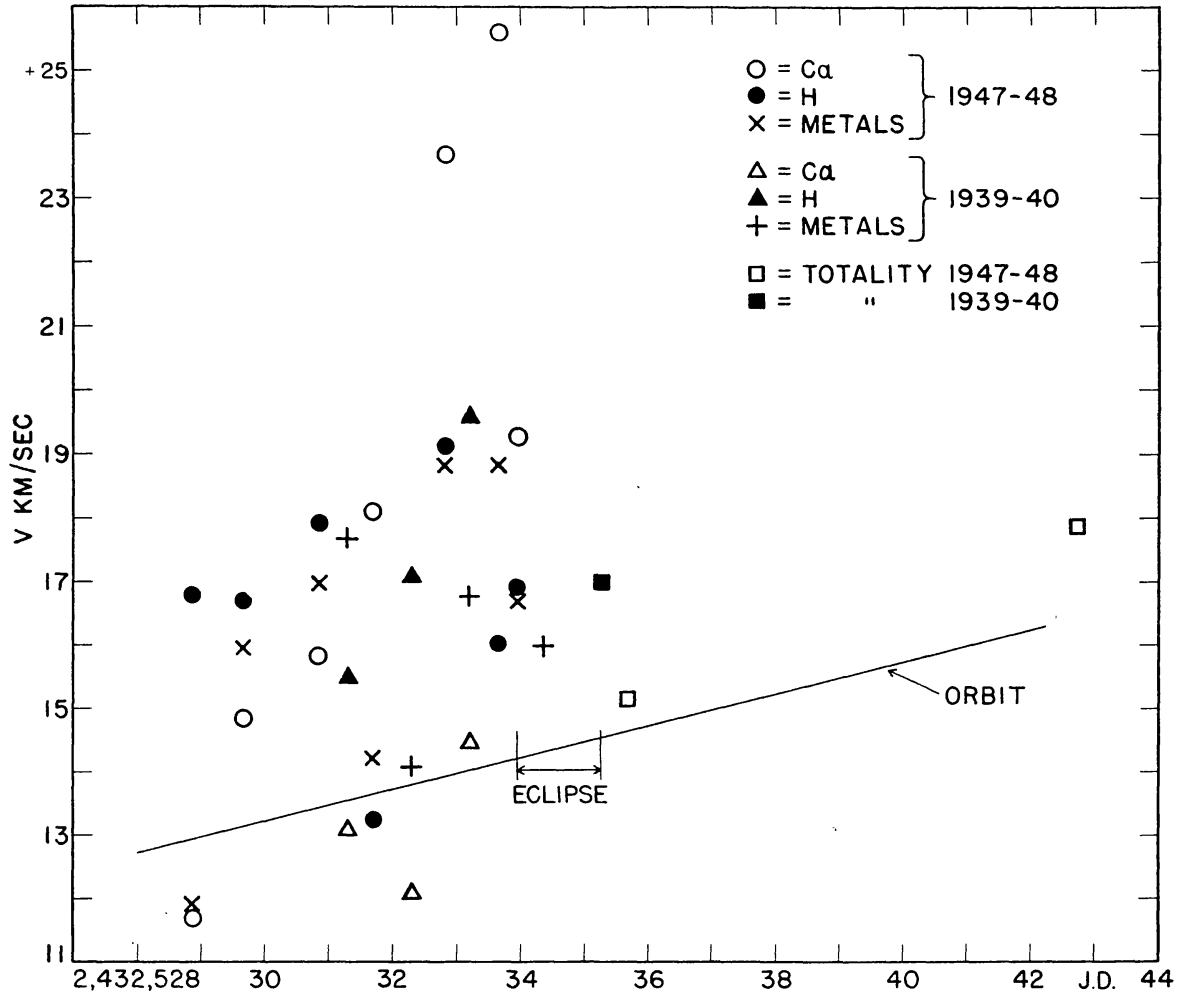

FIG. 10.—Radial velocities near ingress

Variations in velocity can be quite rapid. Note the two 1947 *Ca* II velocities nearest ingress. These are from plates taken only 7 hours apart, and the difference of about 6 km/sec is too large to be accidental.

In general, the hydrogen and metal velocities agree moderately well, with *Ca* II showing the most outstanding deviations, but always in the lower levels where the H and K lines are strong and almost square-sided. This behavior might be explained qualitatively as follows: Suppose that all the lines are really composite, made up of a number of overlapping components distributed in some manner about the mean wave length. Now, if the individual components of the H and K lines are themselves fairly strong,

[10] The JD scales of Figs. 10 and 11 are for the 1947–1948 eclipse. The points for 1939–40 were brought up to date by adding three periods of 972.16 days.

saturated lines, the accidental addition of such a component near one edge of the composite line can introduce an appreciable shift of the mean. If, however, the individual components of the metallic lines and, to a somewhat lesser extent, of the hydrogen lines are quite weak, the accidental addition of an off-center component will have a very much smaller effect on the mean.

That the foregoing explanation is probably correct is shown by careful comparator examination of K on plates 5011 and 5015. When the metallic lines are brought into

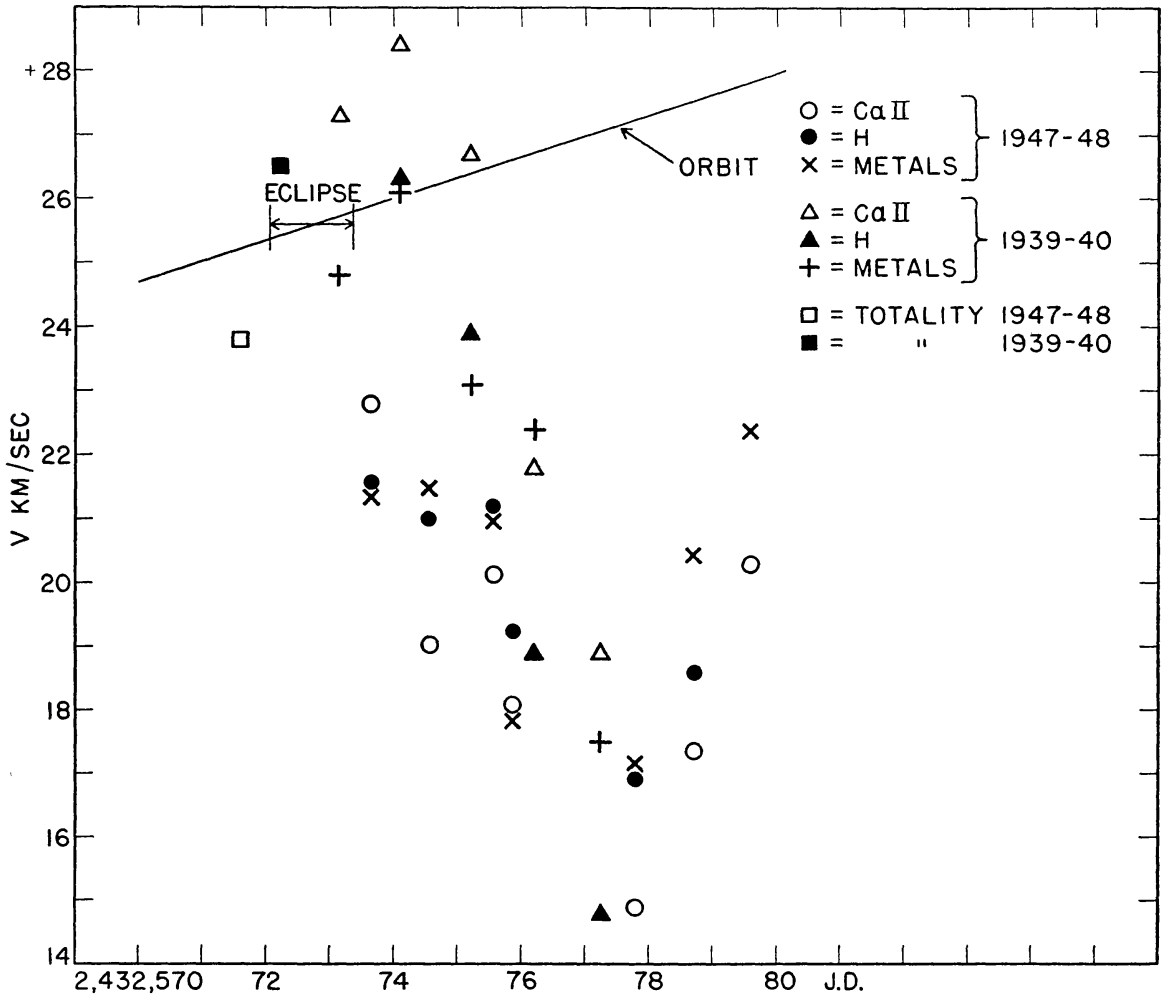

FIG. 11.—Radial velocities near egress

coincidence on these two plates, the violet edges of the two K lines also coincide, but the red side of K on 5015 has a slight redward extension not shared by the line on 5011. This effect, unfortunately too small to show on a reproduction, is qualitatively similar to those found recently in 31 Cygni,[11] where the K line has been observed to break up into distinct components. It is probable that much the same thing occurs in Zeta Aurigae but that the deviations of the components from the mean wave length are smaller in this star than in 31 Cygni.

Whatever the physical significance of the chromospheric radial velocities may be, variations in them do not seem to have much to do with chromospheric extension. Note that, except for the two large deviations of *Ca* II previously mentioned, the maximum

[11] A. McKellar, G. J. Odgers, L. H. Aller, and D. B. McLaughlin, *Nature*, 169, 990, 1952.

deviations of the 1947–1948 ingress are only about half the deviations at egress. Yet the 1947–1948 ingress is the one transit of the four discussed here which differs from the others in the direction of greater chromospheric extension.

V. INTERPRETATION

a) SPECTROSCOPIC AND PHOTOMETRIC GRADIENTS

It is perfectly clear now that the chromospheres of stars like the K component of Zeta Aurigae are complex structures, far indeed from a state of simple hydrostatic equilibrium. A goodly portion of this complexity is no doubt inherent in the nature of the K star, but, in considering the problem as a whole, it must be remembered that the presence of the hot companion will introduce effects which would not be present, were the K star alone in space. The radiation of the companion, for instance, is likely to play a more or less complicated role in determining the physical state of at least the outer

TABLE 9

SPECTROSCOPIC LOGARITHMIC APPARENT GRADIENTS, $\Delta \ln N/\Delta h$, AT $h = 10 \times 10^6$ KM AND $h = 40 \times 10^6$ KM

ELEMENT	$\Delta \ln N/\Delta h$ (CM^{-1})			
	$h = 10 \times 10^6$ Km		$h = 40 \times 10^6$ Km	
	A*	B†	A*	B†
H‡	~0	~0	1.2×10^{-12}	0.5×10^{-12}
Ca I	12.7×10^{-12}	9.9×10^{-12}	.....	.....
Ca II	6.0×10^{-12}	3.9×10^{-12}	1.3×10^{-12}	0.6×10^{-12}
Fe I	4.4×10^{-12}	3.7×10^{-12}	.....	.....
Mn II	3.7×10^{-12}	2.8×10^{-12}	1.0×10^{-12}	0.6×10^{-12}
Fe II	4.2×10^{-12}	2.8×10^{-12}	1.2×10^{-12}	1.0×10^{-12}

* Ingress and egress, 1939–1940; egress, 1947–1948.
† Ingress, 1947–1948.
‡ Population of first excited level.

atmospheric layers of the K star. Thus a complete solution of the problems presented by the eclipse phenomena of Zeta Aurigae would doubtless necessitate a careful disentangling of the inherent properties of the chromosphere of the K star from those which are induced by the presence of the companion.

We must confess at the outset that a successful, comprehensive interpretation of the observations has eluded us. This lack of success is not too surprising in view of the fact that many aspects of the solar chromosphere, which is much more accessible to observation than that of Zeta Aurigae, still present unsolved problems. Nonetheless, in this section we wish to discuss some of the observed phenomena, even though the net result may be nothing more than a clarification of the difficulties encountered.

A comparison of the spectroscopic atmospheric gradients with those found from photometric measures is the first item for consideration. In Table 9 are given the logarithmic gradients, $\Delta \ln N/\Delta h$, for some representative particles for the heights 10×10^6 and 40×10^6 km. The lower of these two heights corresponds to a level in the chromosphere just outside the beginning or end of photometric eclipse, while the upper one is, of course, well away from all eclipse effects. The gradients were obtained by drawing the tangents to the curves of Figures 3, 4, 5, 6, and 8 at the heights specified and are given both for ingress 1947–1948 and for the mean of the other three transits.

While no high precision is claimed for the gradients of Table 9, there can be no doubt that the larger differences between the various entries are certainly real, as are also the differences between the columns labeled "A" and "B" at the two heights. The mean ratio, A/B, for $h = 10 \times 10^6$ km, is 1.4, while it is 1.9 for $h = 40 \times 10^6$ km, indicating that ingress 1947–1948 differs from the other transits increasingly with height.

Conversely, the curves of Figures 3–8 suggest that at the heights corresponding to photometric eclipse there is little or no difference in slope between ingress 1947–1948 and the other transits. This result is in agreement with the discussion of the photometric data by Roach and Wood,[12] who find no difference in eclipse gradient between ingress and egress in 1947–1948, although the material bearing on this point is not extensive. The conclusion therefore seems justified that the phenomena which differentiate ingress 1947–1948 from the other transits are restricted to the upper chromospheric heights and do not have much effect in the lower levels corresponding to photometric eclipse. In fact, there is no evidence that any of the derivable parameters—T_{ex}, V_T, or degree of ionization—are different for the abnormal transit, which therefore seems to deviate from the normal ones only in the sense of a slower decrement of density in the upper chromospheric levels.

It would be highly desirable to derive reliable spectroscopic density gradients in the lower chromosphere for comparison with the gradients found from the photometric measures. Reference to Figures 3–8 and to Table 9 shows, however, that this is not a simple straightforward matter. In the first place, different particles show a considerable range in apparent gradient at a height of 10×10^6 km, which is already outside photometric eclipse; and the graphs suggest that these differences probably become even greater at still lower heights. Moreover, all the plots indicate curvature, i.e., nonconstant gradients, so that it is not possible to extrapolate from the outer regions down to the lower levels. Since both the neutral and the ionized metals (excluding *Ca* I and *Ca* II) have similar apparent gradients, it appears that the results for these particles are probably least affected by variable ionization or excitation, and most nearly represent the true rate of change with height of the quantity of matter along successive rays. If this assumption is permissible, then from Table 9 it follows that, for normal transits, in the range of heights corresponding to photometric eclipse,

$$\frac{\Delta \ln N}{\Delta h} > 4 \times 10^{-12} \text{ cm}^{-1}, \tag{2}$$

and the establishment of this inequality is all that can be derived from the spectroscopic data.

In their discussion of the photometric results, Roach and Wood[12] assume that the K-star atmosphere is characterized by a constant density gradient, $n = n_0 e^{-\alpha \Delta h}$, and that the principal source of light-loss in the partial phases is the line absorption of the chromosphere. On the basis of these assumptions they deduce that the parameter α has the value 5.1×10^{-12} cm^{-1}. Our inequality (2) is therefore consistent with this value for α; but a closer comparison does not appear feasible, since our curves for log N versus height are not accurately enough defined at heights below 10×10^6 km.

The steepest of the curves for log Nf versus height (Fig. 3) suggests that the gradient may attain a value such that there is a ratio of about 100:1 in the number of *Ca* I atoms in the line of sight at the inner and outer limbs of the B star. Since the resultant absorption line produced under these circumstances may depend in a complicated way upon the curve of growth, a numerical investigation of the influence of the finite size of the disk of the B star was made for these extreme conditions. Three cases were considered in which the values of log Nf at the inner and outer limbs were taken to be, respectively, 10^{19} and 10^{17}; 10^{18} and 10^{16}; 10^{17} and 10^{15}. The disk of the B star was then divided into

[12] *Ann. d'ap.*, 15, 21, 1952.

ten segments of equal area, and the contour of the absorption line produced by each segment was calculated by means of the standard formulae, using in each case the value of Nf corresponding to the distance of the segment from the limb. The ten lines from the segments were then added together to form the resultant calculated line whose area was measured with a planimeter, and the corresponding log Nf was read from an appropriate curve of growth.

From the results of this procedure given in Table 10, it is clear that even with the rather extreme assumed gradient and for values of Nf extending from the flat part of

TABLE 10

EFFECT ON LOG Nf OF FINITE SIZE OF B STAR FOR RATIO OF 100:1 FROM INNER TO OUTER LIMB

Log Nf at Limbs	Log Nf at Center of Disk	Log Nf from Composite Line
19–17	18.00	18.18
18–16	17.00	17.18
17–15	16.00	16.18

the curve of growth well into the square-root portion, the effect of the finite size of the B-type star is small and does not produce errors in log Nf in excess of 0.2. For weaker lines the effect will be still less; and we conclude, therefore, that none of the apparent gradients in Figures 3–8 are appreciably influenced by the finite size of the B star.

b) IONIZATION IN THE CHROMOSPHERE

The preceding section on gradients remains seriously incomplete in one major aspect. Although it has been established that the observed apparent gradients are probably fairly reliable and that the major differences between them (Figs. 3–8) are real, no reasons for these differences have been adduced. There are only two ways of accounting for differences in apparent gradient, and these need not, of course, necessarily be mutually exclusive. The first is to suppose that the various particles comprising the chromospheric material do not all have the same density distribution with height. In view of the well-established turbulent nature of the chromosphere, however, one would naturally be predisposed to consider it well mixed throughout and would not look with favor upon a hypothesis requiring a variety of density distributions. The alternative is to ascribe the observed gradient differences to the influence of ionization or excitation or both. In this section we shall inquire briefly into these and related questions.

We cannot proceed at this point without making some simplifying assumptions. First, because the neutral and ionized metals (again excepting *Ca* I and *Ca* II) all have similar apparent gradients, we shall assume that these particles indicate the true chromospheric density gradients. Thus at the lower heights, within the range of photometric eclipse, we shall adopt a value of $\alpha = 5 \times 10^{-12}$ cm^{-1}, while in discussions of higher levels well outside photometric eclipse we shall use $\alpha = 1 \times 10^{-12}$ cm^{-1}. These values are suggested by the data for the "normal" eclipses (see Table 9), and α is the quantity which appears in the density-distribution equation

$$n = n_0 e^{-\alpha \Delta h} . \tag{3}$$

In calculations of ionization we shall use throughout, for all particles, the simplified expression,

$$\frac{n_i n_e}{n_0} = 10^{15.4 - \vartheta I} T_* T_e^{1/2} W . \tag{4}$$

In equation (4) ϑ is $5040/T$, I is the ionization potential in volts, T_* is the temperature of the radiation falling on the matter, T_e is the local electron temperature, and W is the geometrical dilution factor for the radiation. In case the ionizing radiation is weakened by penetrating an optical thickness τ, a factor $e^{-\tau}$ may be applied to the right-hand side of equation (4).

It is first necessary to deduce approximate values of density, and at this point we immediately encounter a difficulty. Only for calcium, and even here only in the lower levels, do we have actual values of N for more than one stage of ionization.

Thus, taking the height 8×10^6 km as a representative "low" level, we find from Figures 3 and 4 $\log N = 16.3$ for *Ca* I and 17.8 for *Ca* II. We do not know what fraction, if any, of the calcium along this ray is doubly ionized. If we assume that none of it is in the form *Ca* III, then the total number of all calcium atoms and ions along the ray is given by $\log N\ (Ca) = 17.8$. In the sun the most recent revision of abundances by Greenstein[13] indicates a hydrogen-to-calcium ratio of $10^{5.6}$. Accordingly, if the same abundance ratio holds in Zeta Aurigae, the number of hydrogen atoms per square centimeter along the ray at height 8×10^6 km should be $\log N\ (H) = 23.4$. Along this ray the observed number in the second state is (Fig. 5) $\log N\ (H_2) = 15.9$; and comparison with the total number leads, by means of the Boltzmann factor, to a mean excitation temperature for hydrogen of 6800°. If any appreciable fraction of the hydrogen along the ray is ionized, an even higher excitation temperature would result. In any case, the mean excitation temperature for hydrogen cannot be so low as that for the metals, which is about 3500° for the ray in question (Fig. 2). For this temperature and with the observed $\log N\ (H_2)$, the total number of hydrogen atoms on the ray would be given by $\log N\ (H) = 30.6$. This number is so large that the chromosphere would be completely opaque at the height in question, because of Rayleigh scattering by neutral hydrogen atoms.[14] Incidentally, the extreme sensitivity of $\log N\ (H_2)$ to the excitation temperature provides the simplest explanation of the difference in shape between the apparent gradient-curve for hydrogen (Fig. 5) and those for the neutral and ionized metals. Only a modest drop in the mean excitation temperature for hydrogen in the lower levels is necessary to account for the flattening of this curve at the lower heights.

Hence, lacking any better procedure, we shall adopt for the ray at 8×10^6 km the values $\log N\ (H) = 23.4$ and $\log N\ (Ca) = 17.8$. These total numbers are related approximately to the central densities on the ray through the expression

$$n_c = N\left(\frac{a}{2\pi R}\right)^{1/2}. \tag{5}$$

With $a = 5 \times 10^{-12}$ cm^{-1} and $R = 1.4 \times 10^{13}$ cm, we find $\log n_c\ (H) = 10.8$ and $\log n_c(Ca) = 5.2$. These would be the numbers of particles per cubic centimeter at the center of the ray if the matter were distributed smoothly according to the density distribution $n = n_0 e^{-a\Delta h}$.

The solar hydrogen-to-iron ratio[13] is $10^{4.9}$, and, if this ratio also holds for Zeta Aurigae, the expected total number of iron atoms and ions along the ray at height 8×10^6 km would be $\log N(Fe) = 18.5$. From Figure 6 we see that the number of atoms active in producing λ 3720 of *Fe* I at the height 8×10^6 km is $\log N = 14.0$. The most recent determination of the absolute f-value for this line[15] is 0.043, from which we deduce that

[13] *Physics for the Engineer* (in press).

[14] See discussion of this point by B. Strömgren, in G. Kuiper, O. Struve, and B. Strömgren, *Ap. J.*, **86**, 570, 1937. Equation (50) of this paper gives the scattering coefficient for neutral hydrogen,

$$\sigma_H = 1 \times 10^{-27}\left(\frac{5000A}{\lambda}\right)^4.$$

[15] H. Kopfermann and G. Wessel, *Zs. f. Phys.*, **130**, 100, 1951.

the number of neutral iron atoms on the ray is log $N(Fe\,\text{I}) = 15.8$. Comparing the expected total number with the observed number of neutral iron atoms, we find that the mean ionization of iron must be fairly high, $N(Fe\,\text{II})/N(Fe\,\text{I}) \sim 500$. In contrast, the mean ionization of calcium at the same height is much lower; in fact, from Figure 9, it is about $N(Ca\,\text{II})/N(Ca\,\text{I}) = 10$, even though the ionization potentials of *Fe* and *Ca* are 7.86 and 6.09 volts, respectively.

In comparing the ionizations of iron and calcium in the lower chromosphere, all the evidence indicates that it is the ionization of calcium which is anomalous. Thus the lines of *Fe* II are, in general, fully as strong as those of *Fe* I, even though the *Fe* II lines arise from levels with excitation potentials between 1 and 2 volts. Again, the lines of *Ti* II (I.P. = 6.8 volts) are generally stronger than those of *Fe* I, and no lines of *Ti* I are observed. Since *Ti* is probably about one hundred times less abundant[13] than *Fe*, this observation would imply that the *Fe* I lines are produced by only a small fraction of the total number of iron atoms. Hence we must conclude that, at the lower chromospheric heights, the ionization of the metals, except for *Ca*, is nearly complete. Furthermore, because of the general parallelism of the neutral and ionized log N versus height–curves, plus the definite result from iron (Fig. 9), we also conclude that the ionization of the metals, again with the exception of calcium, does not change appreciably with height over the range to which the neutral particles may be followed.

Is it possible to account for the curious "collapse" of the calcium ionization in the lower chromospheric levels? Presumably, the calcium is ionized by the radiation of the B-type star, and one would therefore expect that a radical change in ionization could result only from some large screening effect at the wave length corresponding to the ionization potential. For *Ca* this wave length is about 2040 A, and there seem to be no unusually strong absorption features in this neighborhood to cut off the radiation of the B-type star. Moreover, other elements of about the same ionization potential might reasonably be expected to be influenced in the same manner. Unfortunately, *Al* (I.P. = 5.96 volts) is the only element for which such a comparison may be made. The resonance lines of *Al* I at λ 3691 and λ 3944 appear in fair strength in the lower chromospheric levels. Although their intensities were not measured, they have been carefully compared with neighboring *Fe* I lines of similar strength, with the result that there can be little, if any, difference in gradient between *Al* I and *Fe* I, whereas if *Al* behaved as *Ca* does, one would expect a much steeper gradient for the *Al* I resonance lines, in analogy with λ 4227 of *Ca* I. Hence we must conclude that the anomalous behavior of calcium is probably not due to effects which might work on any element of similar ionization potential but is caused by something peculiar to calcium itself. We shall return to this point later.

Figure 9 shows that the ionization of calcium rises with height and appears to approach a value of log $N(Ca\,\text{II})/N(Ca\,\text{I}) \sim 3.4$ in the higher chromospheric levels, corresponding to $N(Ca\,\text{II})/N(Ca\,\text{I}) \sim 2500$. If we assume that this degree of ionization corresponds to the constant ionization of the other metals, we may legitimately compare the calcium and iron ionizations in the higher levels by means of equation (4). From the latter we have

$$\frac{N(Fe\,\text{II})/N(Fe\,\text{I})}{N(Ca\,\text{II})/N(Ca\,\text{I})} = 10^{-\vartheta(I_{Fe}-I_{Ca})} = 10^{-8900/T}. \qquad (6)$$

The left-hand side of equation (6), from the preceding discussion, is 0.20; the right-hand side is 0.26 or 0.18 for $T = 15{,}000°$ and $12{,}000°$, respectively. A temperature of 12,700° for the ionizing radiation gives exact agreement; but this whole procedure is rather crude, and no great weight should be given to this particular value. However, the general consistency attained thus far may give a little confidence in some of the assumptions which have necessarily been made.

Finally, assuming our value for the ionization of iron, $N(Fe\ \text{II})/N(Fe\ \text{I}) \sim 500$, to be correct, we may derive an estimate for the mean electron density from equation (4). The dilution factor for the radiation of the B-type star is $W = 3 \times 10^{-6}$, and we take $T_e = 4000°$ and $T_* = 15{,}000°$. Then from equation (4) we find $n_e = 3.6 \times 10^{10}$, which is approximately equal to the central hydrogen density on the ray found earlier. The implication in this result is that the hydrogen is also fairly heavily ionized throughout, and, if so, it is not clear how there can be enough neutral hydrogen to account for the strong Balmer line absorption. Before accepting these results it is necessary to examine the penetration of the ionizing radiation into the chromosphere.

c) APPLICATIONS OF STRÖMGREN'S THEORY

In a discussion of ϵ Aurigae, B. Strömgren[14] has developed methods of dealing with the ionization produced in the atmosphere of a large, cool star by radiation from a small, hot companion. In this section we shall make use of Strömgren's analysis to see whether it will further our understanding of the chromospheric structure of Zeta Aurigae. The geometrical arrangement is sketched in Figure 12. Briefly, Strömgren shows that, along a given ray from the B-type star, hydrogen will be almost completely ionized up

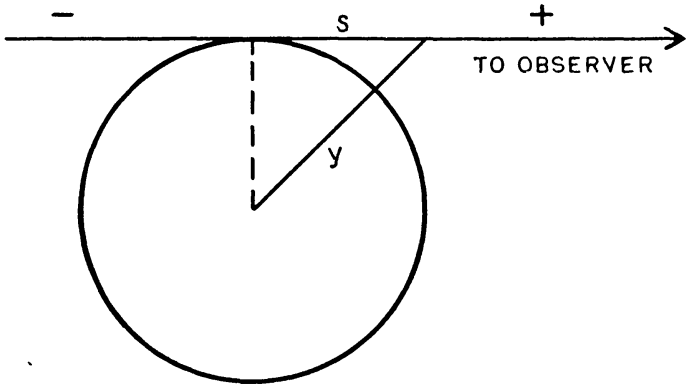

FIG. 12.—Geometry of Strömgren's analysis. The quantity t in the formulae is s/y

to a certain point. Then the ionization will drop very rapidly, owing to depletion of the ionizing quanta, to a value close to zero, which will persist along the remainder of the ray.

The position of the boundary, t_H, between the ionized and neutral zone (H II and H I regions) is given by

$$1 = \frac{a_H}{C_H} (n_c)^2 \left(\frac{\pi R}{a}\right)^{1/2} \tfrac{1}{2} [1 + \phi (t_H \sqrt{[aR]})], \tag{7}$$

where a_H = continuous absorption coefficient of hydrogen at the Lyman limit = 6.3×10^{-18} cm^2; $C_H = 10^{15.4-\vartheta I} T_* T_e^{1/2} W$; R = radius of K-type star = 1.4×10^{13} cm; a = gradient = 5×10^{-12} cm^{-1} in the lower chromosphere, and ϕ is the probability integral,

$$\phi (x) = \frac{2}{\sqrt{\pi}} \int_0^x e^{-x^2} dx .$$

For $T_* = 15{,}000°$, $T_e = 4000°$, and $W = 3 \times 10^{-6}$, we find $C_H = 2.2 \times 10^{11}$.

To find, for any ray, the fraction of total hydrogen atoms contained within the ionized zone, Strömgren's equations may be slightly generalized. Thus the number of ions along the ray is given by

$$N_i = \int_{-\infty}^{t_H} n dt = n_c \left(\frac{\pi R}{2a}\right)^{1/2} [1 + \phi \{t_H \sqrt{(\tfrac{1}{2} aR)}\}], \tag{8}$$

in which the value of t_H found from equation (7) is to be used, whereas the total number is given by

$$N_{\text{tot}} = \int_{-\infty}^{\infty} n\,dt = n_c \left(\frac{2\pi R}{a}\right)^{1/2}. \tag{9}$$

From equation (7), with the above values of the parameters and with $\log n_c = 10.8$ as found in the preceding section, we find $t_H(aR)^{1/2} = -3.21$. Then from equations (8) and (9) it follows that, for the ray at height 8×10^6 km, on the assumption of a smooth distribution of matter, only a small fraction of the hydrogen on the ray is ionized. In fact, we find $N_i/N_{\text{tot}} = 7 \times 10^{-4}$. In other words, the zone of highly ionized hydrogen extends inward only a short distance, and practically all the hydrogen on the ray is neutral, less than one-thousandth of it lying within the *H* II zone.

Returning to equation (7), that ray for which the ionization just extends through the atmosphere, the critical ray, is the one for which $t = +\infty$. Hence the central density on the critical ray is

$$(n_c)^2_{\text{crit}} = \frac{C}{a}\left(\frac{a}{\pi R}\right)^{1/2}. \tag{10}$$

For hydrogen, using the same numerical values as before, $(n_c)_{\text{crit}} \sim 10^8$. If we lump the metals together, taking the mean ionization potential to be 7.5 volts, the resulting central density on the critical ray is about 10^9. In making this last calculation, the continuous absorption coefficient for the average metal has been assumed equal to that of hydrogen, for want of more accurate information. The significance of the critical ray is that, for rays with lower central density than $(n_c)_{\text{crit}}$, the region of high ionization extends completely through the atmosphere; for rays with larger n_c, there is a nonionized region whose extent is given by equation (7).

The various values of $\log N$ and $\log n_c$ which have been deduced thus far on the assumption of a smooth density distribution are minimum values, since they are all based on the assumption of no *Ca* III along the ray under discussion at height 8×10^6 km. The minimum value of n_c for hydrogen, $\log n_c = 10.8$, is much larger than the critical central density, and, as we have seen, practically all the hydrogen on the ray should be neutral. The hydrogen-to-metal ratio is presumably of the order of 6000; thus $\log n_c$ for the metals would be about 7.0, which is much below the critical value for an ionization potential of 7.5 volts, namely, 9.0. Hence, along the ray in question, practically all the electrons must come from the metals, all of which should be highly ionized everywhere on the ray. We must next inquire how high the degree of metal ionization is. For this purpose we make use of iron, for which $\log n_c = 5.9$ if the solar abundance ratio of hydrogen to iron is applicable in Zeta Aurigae.

Let us suppose that about 10 per cent of the metal atoms are iron. Then $n_e = 10n(Fe)$, and we find from equation (4), for the center of the ray,

$$\left(\frac{n_i}{n_0}\right)_{Fe} = 10^{6.3}.$$

The ionization at the center of the ray should be a minimum, since the density there is maximum. Hence even the minimum calculated ionization of iron is greatly in excess of the mean value deduced from observation on the basis of no *Ca* III. Clearly, something is basically wrong, and there seem to be two ways out of the difficulty: either all our values of N and n are too small by a factor of about 10^4, or we must give up the smooth distribution altogether and assume that the chromospheric material occurs in condensations of sufficiently high density to yield a reasonable degree of ionization.

The first of these alternatives can be eliminated at once, in the following manner. Let us take for the central calcium density on the ray a value 10^4 times greater than was

found before, i.e., log $n_e(Ca) = 9.2$, and calculate the boundary between the *Ca* III and *Ca* II zones by means of equation (7). For this purpose we make use of the value of the continuous absorption coefficient of *Ca* II, $a_{Ca\,II} = 2.4 \times 10^{-19}$, computed by Bates and Massey.[16] The result is that the *Ca* III zone extends less than halfway along the ray; hence there should have been more than 10^3 as much calcium in the form *Ca* I and *Ca* II as was observed. This argument seems to dispose of the possibility of a smooth distribution with the density increased by 10^4.

d) CHROMOSPHERIC CONDENSATIONS

We are thus forced to give up the idea of a smooth distribution of chromospheric material and must consider a model in which the matter occurs in condensations of some kind. In order to attain some approximation to the nature of the condensations, we shall suppose them to be all alike as to size and density and, further, that the observed or deduced degrees of ionization are those which apply within each condensation.

If we now compare a ray which traverses a given amount of smoothly distributed hydrogen with a ray passing through the same total amount but in which the hydrogen is collected into condensations, we conclude as follows: the ray passing through the condensations will have suffered a larger depletion of ionizing radiation because a larger proportion of the hydrogen in the condensations is neutral, owing to their higher density. Hence, as in the smooth distribution, practically all the hydrogen on the 8×10^6-km ray should be neutral also in the nonsmooth distribution. This means that practically all the electrons in the condensations must come from single ionization of the metals.

We have seen that for $T_* = 12{,}700°$ the ionization of *Ca* and of *Fe* agrees in the higher levels. With this value of T_*, one finds from equation (4) that $n_e = 10^{10}$, in order to give the proper degrees of ionization for these elements. Hence $n(M) = 10^{10}$ also, where $n(M)$ is the number of metal atoms per cubic centimeter, and, with a hydrogen-to-metal ratio of 6000, $n(H) = 10^{13.8}$ cm^{-3}. The condensations have thus turned out to be surprisingly, even uncomfortably, dense. They must also be quite small, since, for a total number of hydrogen atoms $10^{23.4}$ per square centimeter and a condensation density of $10^{13.8}$ per cubic centimeter, only $10^{9.6}$ cm of the path can be occupied. In order that there may be enough condensations in the line of sight to account for the curve of growth, say, of the order of 10–100, it follows that the thickness of the condensations in the line of sight can be only a few hundred to a few thousand kilometers at most. The shape of the condensations cannot, of course, be specified. They might be thin sheets of large width compared to their thickness, or they might be thin, more or less round, filaments. In any event, their small thickness and high density are reminiscent of some of Menzel's descriptions of the structure of prominences and spicules in the solar chromosphere.[17]

e) RECONSIDERATION OF NUMBERS OF ATOMS

In the light of the results of the preceding section we must now retrace our steps to see whether our basic assumptions concerning numbers of atoms in the line of sight require modification. For the ray at height 8×10^6 km, it will be recalled that the observed value of log N for calcium, log $N(Ca) = 17.8$, led to the result that log $N(H) = 23.4$. Underlying this conclusion were the assumptions that (1) the solar abundance ratios hold also for Zeta Aurigae and (2) no large fraction of the calcium on the ray was in the form *Ca* III. We must now check this second assumption against the specifications of the condensations deduced above.

With $T_* = 12{,}700°$, $T_e = 4000°$, and log $n_e = 10$, equation (4) yields the result $n(Ca\,III)/n(Ca\,II) = 12.5$. In other words, over 90 per cent of the calcium in the con-

[16] *Proc. R. Soc. London, A*, **177**, 281, 1941.

[17] D. H. Menzel, *Our Sun* (Philadelphia: Blakiston Co., 1949), chap. viii.

densations should exist as *Ca* III, and all the values of N based upon the observed value of log $N(Ca)$ should be increased by a corresponding factor. Such a change would be disastrous for the ionization computations. For instance, we should have $N(Fe\,\text{II})/N(Fe\,\text{I}) \sim 5000$ instead of 500, while $N(Ca\,\text{II})/N(Ca\,\text{I}) = 2500$ in the higher levels would remain as before, since it is an observed ratio. Before accepting this revision, let us consider the rather special circumstances surrounding the ionization of *Ca* II to *Ca* III.

The second ionization potentials of all the common metals except calcium exceed that of hydrogen. Hence, if the ray we are considering lies principally within the *H* I zone, all these metals except calcium are protected from second ionization by the radiation from the B-type star by the continuous absorption of hydrogen, which removes practically all the radiation lying above 13.54 volts. Since the second ionization potential of calcium is only 11.82 volts, it appears inevitable at first glance that most of the *Ca* II will be ionized to *Ca* III.

A second consequence of the neutrality of most of the hydrogen is, however, that the Lyman absorption lines will be tremendously strong over most of the ray, and we note that the principal *Ca* II absorption edge at 11.82 volts is only 19 A redward from Ly-β. Is it possible that the ionization of *Ca* II to *Ca* III is suppressed in the lower atmospheric levels by the presence of Ly-β?

The absorption coefficient in the wing of a line is given by[18]

$$k = 16.5 \times 10^{-26} \left(\frac{\lambda}{\Delta\lambda}\right)^2 f . \tag{11}$$

With $\lambda = 1029$ A, $\Delta\lambda = 19$ A, and $f = 7.9 \times 10^{-2}$, we find from equation (10) that $\tau = 3.84 \times 10^{-23} N$. Hence for log $N(H) = 23.4$ it follows that the opacity due to Ly-β is adequate to suppress the ionization of *Ca* II over about three-fourths of the light-path. When we consider that the numbers which have gone into this computation are fairly uncertain and that the opacity increases by a factor of nearly 2 by moving only 5 A shortward of the absorption edge of *Ca* II, it seems very probable that little *Ca* III will exist on the ray at height 8×10^6 km. If this argument is allowed, it follows that our estimates of $N(H)$ and $N(Fe)$ for this ray are essentially correct as given previously.

The foregoing discussion clarifies another puzzling observational point which has not hitherto been mentioned. Consider the curves of log N versus height in Figures 4 and 8. For the normal eclipses, between the heights 8×10^6 and 40×10^6 km, log N for *Ca* II decreases by 4.5, while the corresponding decrease for *Fe* II is only 2.9. This difference is not likely to mean that the relative abundances of calcium and iron change with height. It is, however, of the right order of magnitude to be accounted for if most of the calcium is in the form *Ca* II at the lower level and over 90 per cent of it exists as *Ca* III at the upper level, while the second ionizations of the other metals remain negligible. This last point requires investigation, since it might be supposed that eventually a height will be reached where the other metals would no longer be screened by the continuous absorption of hydrogen. With our specifications for the condensations, we find that this does not happen. From equation (4), with a hydrogen density of $10^{13.8}$, it follows that the ionization of hydrogen never exceeds about 5 per cent. Hence, without appreciable error, we may write, for the opacity at the Lyman limit,

$$\tau_{\text{Ly}} = L \times 10^{13.8} \times 6.3 \times 10^{-18} , \tag{12}$$

where L is the path length in centimeters. In order that τ_{Ly} may attain a value of 10, it follows that $L = 10^{4.4}$ cm. Thus less than 1 km of path length is required to provide virtually perfect screening against second ionization for metals such as iron. Hence in a condensation exposed to the full radiation of the B-type star, only a negligible fraction of the metals other than calcium will be doubly ionized.

[18] A. Unsöld, *Physik der Sternatmosphären* (Berlin: J. Springer, 1938), eq. (41.6).

f) CONTINUOUS ABSORPTION

The ray at height 8×10^6 km lies just within the range of heights included in the photometric eclipse, and we must next investigate the continuous opacity of the chromospheric material, since any model of the chromosphere must, of course, be consistent with the photometric results as well as with the spectroscopic observations. If the matter is in the form of condensations with neutral hydrogen and singly ionized metals, the only type of opacity which requires consideration is that due to negative hydrogen. Moreover, since we are assuming that all the condensations are alike, we need deal only with a uniform layer whose physical characteristics are the same as those of the condensations and whose thickness is such that the amount of matter per square centimeter is the same as that given by the spectroscopic observations. We therefore inquire into the continuous opacity of a layer in which there are $10^{13.8}$ neutral hydrogen atoms per cubic centimeter; $10^{23.4}$ neutral hydrogen atoms per square centimeter; and a hydrogen-to-metal ratio of 6000, with the metals all singly ionized, and therefore $n_e = 10^{10}$.

The ionization potential of H^- is 0.75 volt, and its ionization will therefore be governed by the radiation from the K-type star.[19] With a dilution factor $W = \frac{1}{2}$ for the K-type star, the Saha equation for negative hydrogen becomes

$$\frac{n_H n_e}{n_{H^-}} = 10^{15.7-\vartheta I} T^{3/2}, \tag{13}$$

where we have set $T = T_* = T_e = T_K$. Assuming the values $T_K = 3200°$, $n_H = 10^{18.8}$, and $n_e = 10^{10}$, we find from equation (13) that $n_{H^-} = 10^4$. Thus, since conditions are uniform in the layer under consideration, $N_{H^-} = N_H(n_{H^-}/n_H) = 10^{13.6}$, and this is the total number of negative hydrogen ions per square centimeter through the layer. At λ 4500 the absorption cross-section for H^- is approximately[20] 3×10^{-17} cm^2; therefore, the opacity at this wave length produced by H^- is only 1.2×10^{-3}.

We conclude that, according to the present chromospheric model for Zeta Aurigae, the major part of the photometric eclipse is, in fact, caused by line absorption, as suggested by Roach and Wood.[12] Only when the line of sight passes through about one hundred times as much material as at the 8×10^6-km level will the H^- opacity begin to play a role. For a gradient of 5×10^{-12} cm^{-1}, the amount of matter in the line of sight would be increased one hundred fold over that at 8×10^6 km at a height of -2×10^6 km, i.e., at a level below that corresponding to second and third contacts. Even making allowance for the uncertainty in our data and for the fact that the gradient may become appreciably steeper below the 8×10^6-km level, it would seem that H^- opacity is unlikely to play any role except possibly at the very end of partial phase, just prior to the onset of totality.

g) TURBULENCE AND EXCITATION TEMPERATURE

The observed difference in $\Delta\lambda_D$ between the neutral and ionized lines and the rise of excitation temperature with height require brief examination. Can these features be accounted for, even qualitatively, on the chromospheric model developed here? Let us consider these two items in the above order.

It is highly improbable that all the condensations have exactly the same density and hence exactly the same degree of metallic ionization. More likely, these parameters vary over some range, and the values we have deduced in the preceding sections are means of some kind. If, now, the less dense (and perhaps less massive?) condensations tend to

[19] It is easy to show that, for ionization processes requiring less than 3.7 volts, the ionization will be determined by the K-type star. Above this value the B-type star predominates.

[20] S. Chandrasekhar, *Ap. J.*, **102**, 395, 1945. The free-free opacity is negligible at λ 4500.

have somewhat more rapid motions than the denser ones, there should be a tendency for the ionized lines to yield a larger $\Delta\lambda_D$ than do the neutral lines. While this idea can hardly be considered as an explanation of the observed phenomenon, it is at least not unreasonable. Moreover, if the chromosphere were not discontinuous in nature and the neutral and ionized particles were thoroughly mixed, it is very difficult indeed to see how the observed difference in $\Delta\lambda_D$ could exist.

We have seen (Fig. 2) that the measured excitation temperature rises steadily with height, beginning at the lowest observed levels with values of the same order as the effective temperature of the K-type star. This fact suggests that perhaps the excitation temperature in the lower chromosphere is determined by the radiation of the K-type star but that the B-type star plays an increasingly important role in the higher levels.

We first consider the relative effectiveness of collisions and radiative processes in determining the populations of the various states of the metallic ions and atoms. The probability of an excitation by electron collision of a level E volts above the ground state is given approximately by the expression,[21]

$$p_c = 2n_e\sigma^2\left(\frac{2\pi kT}{m}\right)^{1/2} e^{-E/kT}, \tag{14}$$

in which n_e is electron density, σ^2 is the collisional cross-section, and T is the electron temperature. With $n_e = 10^{10}$, $\sigma^2 = 10^{-17}$, and $T = 4000°$, it follows that the probability of collisional excitation of a level of 1-volt energy is $p_c \sim 1$.

The probability of radiative excitation is computed from the usual formula,

$$p_r = B_{12}u_\nu ,$$

where B_{12} is the Einstein absorption coefficient, related to the f-value for the line concerned through the expression

$$B_{12} = \frac{\pi e^2}{mh\nu} f ,$$

and u_2 is the radiation density.

Assuming, now, that both stars radiate as black bodies, so that u_ν is given by the Planck function multiplied by the appropriate dilution factor and that the temperatures of the K-type and B-type stars are 3200° and 15,000°, respectively, one finds, for a line at λ 4000 A,

$$p_r = 3.3 \times 10^3 f \quad \text{for the radiation of the K-type star,}$$

$$p_r = 1.2 \times 10^2 f \quad \text{for the radiation of the B-type star.}$$

The f-values of the stronger metallic lines are of the order of 10^{-2}; hence there is some indication, though it is not decisive, that the excitation temperature of a condensation exposed to the full radiation of both stars would approximate that of the K-type rather than the B-type star. In the higher chromospheric levels there should be appreciable screening of the radiation of the K-type star by the underlying material, together with less screening of the radiation from the B-type star, and a corresponding tendency for the excitation temperature to be governed more by the B-type star and by the electron collisions. Since the velocity distribution of the electrons is determined by the higher temperature radiation, it might be expected that when they make a significant contribution to the excitation temperature, it, too, will be in the direction of higher values. There appears to be at least a possibility, therefore, that the variation of T_{ex} with height might be understandable somewhat along the lines of the foregoing discussion.

[21] O. Struve and K. Wurm, *Ap. J.*, 88, 84, 1938.

h) SUMMARY AND CONCLUDING REMARKS

The picture of the chromosphere of Zeta Aurigae developed here is one of great discontinuity. A ray through the chromosphere passes mostly through empty (spectroscopically speaking) space and encounters here and there a condensation of matter of relatively small size and high density. Relative motion of the condensations will account for the shapes of the curves of growth, i.e., for the "turbulence"; and the size and density of the condensations explain the various ionizations required to bring the spectroscopic observations into agreement with the solar abundance ratios. Moreover, there is no conflict with the photometric observations or with their recent interpretation. Even the differences between abnormal chromospheric transits, such as ingress 1947–1948, and the normal ones receive a simple interpretation. An abnormal transit is simply one in which there are more than the average number of condensations in the line of sight, especially in the higher levels; but the condensations themselves are not observationally distinguishable from those present at other times. Taken as a whole, therefore, the analysis presented here appears fairly successful.

But there is one outstanding failure which we must regard as serious, namely, the fact that we cannot account for the "collapse" of the *Ca* II ionization in the lower chromospheric levels. Our entire analysis is based upon the idea that the degree of ionization in the chromosphere of the K-type star can be calculated by elementary means on the assumption of black-body radiation of the B-type star, with allowance, when necessary, for absorption features introduced by the chromosphere of the K-type star itself. That these simple considerations fail completely to explain the one ratio of ionized to neutral particles which we can observe directly is very unsatisfactory and gives no assurance that our other calculations can lead to useful results. Nevertheless, all the evidence indicates that the ionizations of the other metals do not vary with height, and we have been forced to regard this fact as the more fundamental datum to be explained.

We cannot get out of our difficulty by supposing that the rapid drop in the *Ca* II/*Ca* I ratio marks the height at which the boundary of the *Ca* II zone moves inward from $-\infty$ in the sense of Strömgren's theory. For Bates and Massey give $a = 2.5 \times 10^{-17}$ as the continuous absorption coefficient of *Ca* I; and, with this value for a and the observed number of *Ca* I atoms on the 8×10^6-km ray, $\log N(Ca\ \text{I}) = 16.3$, the total opacity over the entire path is only 0.5, far below what is needed for any appreciable effect on the ionization. Curiously, the *Ca* II/*Ca* I ratio at 8×10^6 km is about that to be expected if the ionization of *Ca* at this level is produced only by the radiation of the K-type star and if $n_e = 10^{10}$. But we are unable to account for the absence of the radiation from the B-type star and must, for the present, regard the behavior of the calcium ionization as an unexplained, and admittedly uncomfortable, phenomenon.

Finally, it must be emphasized that no attempt has been made here to give a *physical* explanation of the Zeta Aurigae chromosphere. Even if the existence of the condensations be accepted, we have no theory as to their origin or their persistence as discrete entities. These problems may very well be quite similar to those presented by many aspects of the solar chromosphere, to which, it seems, there are also no really satisfactory answers at the present time.